Effect of pH on the stability of passivating gel layers formed on International Simple Glass

Maxime Fournier, Thomas Ducasse, Anne Perez, Ayoub Barchouchi, Damien Daval, S. Gin

Effect of pH on the stability of passivating gel layers formed on International Simple Glass

Maxime Fournier[a], Thomas Ducasse[a], Anne Pérez[b,c], Ayoub Barchouchi[a], Damien Daval[b], Stéphane Gin[a]

[a] CEA, DEN, DE2D, SEVT, F-30207 Bagnols sur Cèze, France

[b] LHyGeS, CNRS, Université de Strasbourg, UMR 7517, 1 rue Blessig 67084 Strasbourg, France

[c] LGE, Université Paris-Est, Laboratoire Géomatériaux et Environnement, (EA 4508), UPEM, 77454 Marne-la-Vallée, France

Corresponding author: Maxime Fournier
Postal address: CEA Centre de Marcoule
DEN/DE2D/SEVT/LCLT, Bat. 208
BP 17171
30207 Bagnols sur Cèze Cedex
France
Tel.: +33 466797710
E-mail address: maxime.fournier@cea.fr

Abstract

It has been well established that borosilicate glass dissolves much more slowly in saturated silica solutions than in deionized water. The present study assesses this assertion for the specific case of International Simple Glass, which is a 6-oxide borosilicate glass of nuclear interest, and was altered between pH = 1 and 10.7 at 90 °C. Depending on the reaction stage, aqueous silica can promote either the formation of a passivating gel layer on the glass surface or the precipitation of certain secondary phases at the expense of the passivating gel. In this study, a negligible effect of aqueous silica on glass dissolution at acidic pH is demonstrated, while a marked effect above $pH_{90\,°C}$ = 7 is observed, ensuring better chemical durability of the glass. Conversely, at higher reaction progress and above $pH_{90\,°C}$ = 9.5, the chemical durability of the glass decreases owing to the formation of secondary phases such as hydroxides or zeolites.

Keywords

ISG, nuclear glass, amorphous silica, pH.

35

Graphical abstract

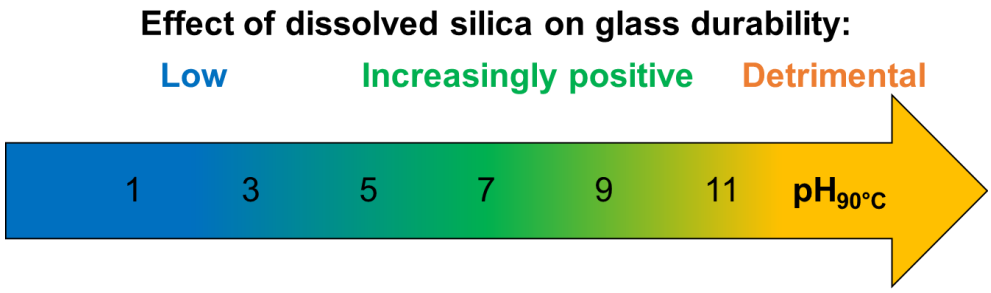

Highlights

- SiO_2(aq) has no effect on the ISG dissolution rate at acidic pH
- Aqueous SiO_2 slows glass dissolution at $pH_{90\,°C} \geq 7$ and low reaction progress
- Aqueous SiO_2 increases glass dissolution at $pH_{90\,°C} \geq 9.5$ and high reaction progress

1. Introduction

Countries such as France, Japan, Russia, India, and Great Britain have chosen to reprocess their spent nuclear fuel. The minor actinides and fission products that arise from this reprocessing are vitrified in borosilicate or, to a lesser extent, phosphate glasses. In France, the vitrified waste form, usually called “nuclear glass,” is packed in carbon steel containers and will eventually be stored in a deep, stable claystone formation with low permeability. Assessment of the safety of the geological repository relies on the performance of various barriers and thus is partly dependent on the chemical durability and radiation resistance of the glass. Although research on the durability of nuclear glass has been ongoing for several decades, it is still a field of intense investigation [1].

In contact with water, glass dissolves and transforms into more stable phases at a rate that is highly dependent on the geochemical conditions. The formation of a Si-rich passivating layer (also called a “gel”) under the most favorable conditions can guarantee a glass package lifetime of several hundred thousand years [2]. For the same glass, the composition and structure of the gel vary depending on environmental parameters, particularly the pH and composition of the solution. A chemical element resulting from the glass dissolution may participate in the formation of the gel and/or the precipitation of secondary minerals, which are thermodynamically more stable but less protective [3-9]. Studies conducted on SON68 and ISG and involving solution spiked in ^{29}Si and ^{18}O have demonstrated that secondary silicate phases form by precipitation of aqueous species, whereas gel forms by in situ hydrolysis/condensation reactions preventing the complete dissolution of silica [10-12]. As an example of competition between gel formation and phases precipitation, some experiments have evidenced gel dissolution reaction at the expense of precipitation reaction of calcium silicate hydrates and zeolites [13, 14]. Finally, thermodynamic data on the gel and secondary phases are of interest for the geochemical modeling of nuclear glasses alteration [15, 16].

The presence of aqueous silica [17-22] has two major effects on glass: on the one hand, it decreases the affinity of the matrix dissolution reaction ($SiO_2 + 2H_2O \rightarrow H_4SiO_4$); on the other hand, it favors the backward reaction of condensation. The latter reaction accounts for the formation of the gel layer, which can, in some circumstances, be transport-limiting [12, 23]. Aqueous silica is not the only dissolved species that can affect the glass durability. In fact, most dissolved species can have an effect, either directly on the hydrolysis reaction of the –Si–O–Si– bonds [24, 25], or indirectly through the pH or the gel formation [6, 26-31]. Because the pH of leaching solutions is generally buffered around 9–9.5 by boron released from the glass ($B(OH)_3 + H_2O \rightarrow B(OH)_4^- + H^+$, $pK_a = 9.14$ at room temperature), and because the pH of many natural groundwaters is in the range of 6–8, many studies have been conducted between pH 7 and 9.5. However, some disposal designs would lead to more alkaline pH conditions [32], raising concerns about the gel stability above pH 9.5. In addition, below pH 7, the role of aqueous silica on the reactivity of glass is unclear.

This study thus reports the dissolution behavior of an international reference glass (International Simple Glass, ISG) [33], which is a 6-oxide borosilicate glass, in solutions that are saturated or unsaturated with respect to amorphous silica at 90 °C for $pH_{90\,°C}$ ranging between 1 and 10.7. Above pH 10.7, it becomes experimentally challenging to saturate the solution due to spontaneous reactions of oligomerization [34]. Two different ratios of the reactive glass surface area to the solution volume (S/V) are considered. These two ratios differ by two orders of magnitude and are complementary over the entire pH range of the study while making it possible to (i) maximize the difference in silica concentrations between a pre-saturated solution and a solution where the silica originates solely from the glass dissolution, and (ii) measure the boron concentration with sufficient analytical precision. More than twenty static tests were conducted over durations up to one year with regular solution sampling. Solid characterization was performed to identify the formation of secondary phases. No specific attention was paid to the passivating properties of the gels formed at various pHs, but previous studies have investigated this aspect, especially at pH 7 and 9 [11,

12, 35-37]. Overall, this study demonstrates that the positive effect of aqueous silica on the durability of ISG is limited to a $pH_{90\,°C}$ range of 7–9.5.

2. Material and Methods

2.1. Preparation of the material

The tests in this study were conducted using ISG; its composition is summarized in Table 1. ISG ingots were prepared by the MO-SCI Corporation (Rolla, MO, USA) [38] and provided by the Savannah River National Laboratory (Aiken, SC, USA). Two different sizes of glass powder were prepared from successive steps of crushing with a vario-planetary mill and sieving to isolate 125–250 µm and 20–40 µm size fractions. The powders were washed to remove fine particles by an iterative decantation process using acetone and absolute ethanol according to Stokes' law.

ISG	SiO_2	B_2O_3	Na_2O	Al_2O_3	CaO	ZrO_2
Oxide wt%	56.2 ± 1.5	17.3 ± 0.9	12.2 ± 0.7	6.1 ± 0.8	5.0 ± 0.6	3.3 ± 0.5

Table 1: ISG composition expressed in oxide weight percent

2.2. Leaching tests

Static leaching tests were performed at 90 ± 2 °C in a perfluoroalkoxy vessel. Two series of tests were conducted: the first (S1) with an S/V ratio of 60 m^{-1} using the 125–250 µm size fraction (0.13 g of glass in 40 mL of solution), and the second (S2) with S/V = 10 000 m^{-1} using the 20–40 µm size fraction (4.25 g in 40 mL). The reactive surfaces correspond to the geometric surfaces by considering the glass grains as spheres, corrected by a factor of 1.3 to take into account the non-sphericity of the glass grains [39].

Leaching tests (Table 2) were conducted in solutions saturated with respect to amorphous silica ("Sat" test series) at various pHs, and in solutions with the same pH but no initial aqueous silica ("Blk" test series). Acid solutions were prepared by diluting nitric acid (65%, Merck Suprapur®) in 18 MΩ·cm ultrapure water, and basic solutions were prepared by

dissolving KOH pellets (Merck Emsure®). The amount of silica introduced to reach saturation at 90 °C in the "Sat" test series was calculated using the Chess code [40]. For $pH_{90\,°C} \geq 9.5$, silica-containing solutions were prepared by dissolving amorphous silica for about a week at 90 °C while stirring. To prepare lower pH solutions, the solution prepared with a $pH_{90\,°C} = 9.5$ was split and acidified. The silica concentration of each solution was checked using a UV-visible spectrometer (Cary® 50 Scan UV-Vis) according to a method analogous to ASTM D859-10 [41]. During the tests, the pH was manually controlled at the set point through regular addition of micro-volumes of concentrated HNO_3 or KOH solutions to counterbalance variations due to glass dissolution or carbonation of solutions.

Test name	Test series	S/V (m^{-1})	T (°C)	$pH_{90\,°C}$	C_{Si} ($mg \cdot L^{-1}$)	Duration (d)
S1-Sat-1	1	60	90	1	$3.1 \cdot 10^2$	365
S1-Blk-3	1	60	90	3	0	365
S1-Sat-3	1	60	90	3	$3.0 \cdot 10^2$	365
S1-Blk-7	1	60	90	7	0	365
S1-Sat-7	1	60	90	7	$1.5 \cdot 10^2$	365
S1-Sat-8	1	60	90	8	$1.8 \cdot 10^2$	365
S1-Sat-9	1	60	90	9	$2.8 \cdot 10^2$	365
S1-Blk-9.5	1	60	90	9.5	0	365
S1-Sat-9.5	1	60	90	9.5	$7.4 \cdot 10^2$	365
S1-Sat-9.8	1	60	90	9.8	$1.4 \cdot 10^3$	365
S1-Blk-10.1	1	60	90	10.1	0	365
S1-Sat-10.1	1	60	90	10.1	$3.9 \cdot 10^3$	365
S1-Sat-10.3	1	60	90	10.3	$1.2 \cdot 10^4$	365
S2-Blk-9.5	2	10 000	90	9.5	0	379
S2-Sat-9.5	2	10 000	90	9.5	$7.4 \cdot 10^2$	379
S2-Blk-9.8	2	10 000	90	9.8	0	379
S2-Sat-9.8	2	10 000	90	9.8	$1.4 \cdot 10^3$	379
S2-Blk-10.1	2	10 000	90	10.1	0	379
S2-Sat-10.1	2	10 000	90	10.1	$3.9 \cdot 10^3$	379
S2-Blk-10.3	2	10 000	90	10.3	0	379
S2-Sat-10.3	2	10 000	90	10.3	$1.2 \cdot 10^4$	379
S2-Blk-10.7	2	10 000	90	10.7	0	379
S2-Sat-10.7	2	10 000	90	10.7	$2.7 \cdot 10^4$	379

Table 2: Characteristics of the "Sat" and "Blk" test series, including the ratio of the glass surface area to the solution volume (S/V), temperature (T), target pH value maintained at 90 °C, initial silicon concentration (C_{Si}), and total duration.

2.3. Solution analyses

Samples of 0.5 mL of solution were removed at 1, 3, 7, 14, and 28 d, 3 months, and 1 y. Samples were ultrafiltered at 10 000 D, acidified with 0.5 N HNO_3, and analyzed using inductively coupled plasma optical emission spectroscopy (ICP-OES, Thermo Scientific iCAP^{TM} 6000 Series) to determine the boron and silicon concentrations. As boron is known to be a glass alteration tracer, the boron concentration was used to calculate the altered glass percentage, %AG, from a mass balance taking into account the change in volume (Equation 1).

$$\%\mathrm{AG} = \frac{C_i(t) \times V(t) + \sum_{j=1}^{t-1} C_i(j) \times V_S(j)}{m \times x_i} \quad (1)$$

where $C_i(t)$ is the mass concentration of element i at time t, x_i is the mass fraction of element i in the glass composition, $V(t)$ is the solution volume at time t, $V_S(j)$ is the volume of the j-th sampling, and m is the mass of the glass.

The equivalent thickness of altered glass, eTh(B), was calculated as a function of time using Equation 2, where r_0 is the glass particle radius at $t = 0$, and r_t is the radius at time t.

$$\mathrm{eTh(B)} = r_0 - r_t = r_0 \times \left[1 - (1 - \%\mathrm{AG})^{\frac{1}{3}}\right] \quad (2)$$

2.4. Solid analyses

X-ray diffraction (XRD). XRD patterns of the altered glass powders were acquired with a Phillips X'PERT Pro diffractometer equipped with a Cu-Kα monochromatic source (λ = 1.5418 Å) operating at 40 mA, 40 kV in Bragg-Brentano geometry. Scans were taken for 2θ ranges from 4° to 80° with a speed of 0.11°·min^{-1} and a step of 0.017° (2θ) using amorphous silica sample holders. The XRD patterns were processed using the DIFFRAC.EVA v. 4.2 (Bruker) software and compared to reference patterns from the International Center for Diffraction Data PDF-4+ 2018 RDB.

155 *Scanning electron microscopy (SEM).* Solid samples taken at the end of the leaching experiments were rinsed, dried, coated with a carbon deposit, and observed using a Zeiss Merlin scanning electron microscope operated with an accelerating voltage of 15 kV and coupled with a lithium-doped silicon detector for energy dispersive X-ray spectrometry.

3. Results

3.1. S1 test series: low *S*/*V* ratio

In the S1 test series, the pH values were generally maintained at the set values within ± 0.3 pH unit, with the exception of a few cases, especially in the first 10 d of the $pH_{90\,°C}$ = 7 tests where the pH control was the most difficult (Figure A.1). The evolution of the silicon concentration is summarized in Table 3, and the complete results of the solution analyses are presented in Appendix D.

In the “S1-Blk” tests (Figure 1.a-b), the highest altered glass thicknesses are observed at $pH_{90\,°C}$ = 3 (S1-Blk-3), while the lowest are observed at $pH_{90\,°C}$ = 9.5 (S1-Blk-9.5). Between $pH_{90\,°C}$ = 3 and 9.5, the altered thicknesses gradually decrease with increasing pH. Above $pH_{90\,°C}$ = 9.5, the altered glass thicknesses increase and exhibit a sharp variation in the alteration rate between 28 and 91 d. This sharp increase is associated with the precipitation of calcium silicate hydrate-like phases (CSH) [38, 42], as evidenced by the SEM results (Figure 2.a), but which cannot be identified by XRD because of the absence of diffraction peaks.

In the “S1-Sat” tests (Figure 1.c-d), the same evolution of the altered glass thicknesses as a function of pH is observed as in the “S1-Blk” tests: a decrease between $pH_{90\,°C}$ = 3 (S1-Sat-3) and $pH_{90\,°C}$ = 9.5 (S1-Sat-9.5) and an increase beyond that point. However, it should be noted that eTh(B) at $pH_{90\,°C}$ = 3 is slightly larger than at $pH_{90\,°C}$ = 1 (S1-Sat-1). For the tests at $pH_{90\,°C} \geq 9.5$, only the boron concentration of the last sample at 1 y can be measured owing to the high dilution factor necessary for the ICP-OES analyses due to the high silica content of these solutions. This result motivated a second test series conducted at a higher *S*/*V* ratio (Section 3.2). Finally, only small amounts of phyllosilicate-like secondary phases [43, 44] are observed by SEM in these tests (Figure 2.b).

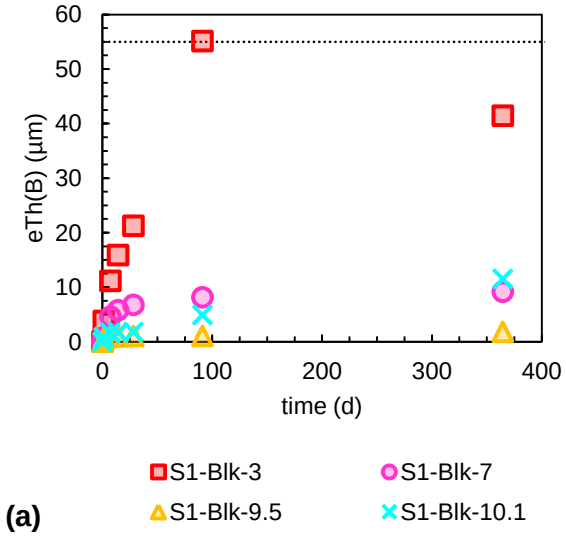
60
50
40
30
20
10
0
eTh(B) (µm)
0
100
200
300
400
time (d)
S1-Blk-3
S1-Blk-7
S1-Blk-9.5
S1-Blk-10.1

(a)

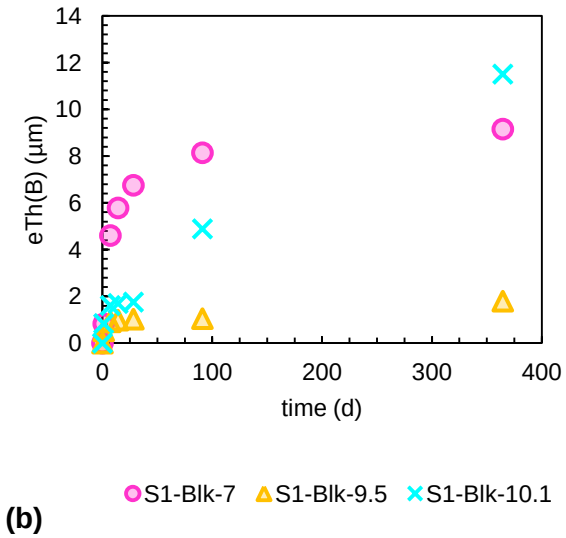
14
12
10
8
6
4
2
0
eTh(B) (µm)
0
100
200
300
400
time (d)
S1-Blk-7
S1-Blk-9.5
S1-Blk-10.1

(b)

185

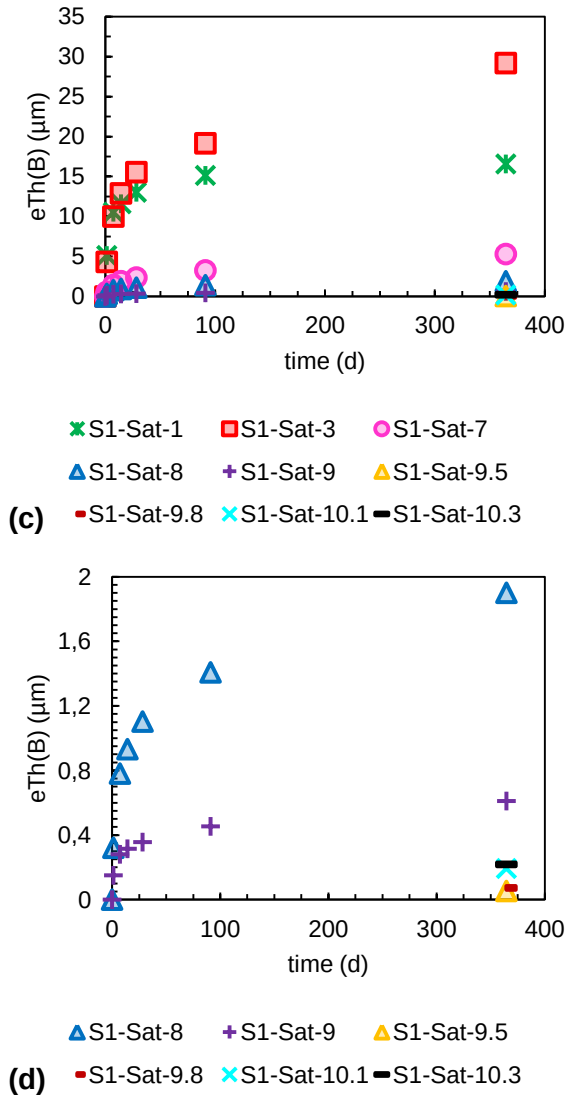

Figure 1: Evolution of the equivalent thickness of altered glass calculated from the boron concentration, eTh(B), for the **(a, b)** S1-Blk and **(c, d)** S1-Sat test series with an *S*/*V* ratio of 60 m^{-1}. The dotted line represents the total alteration of the glass (%AG = 100). Figures **(b)** and **(d)** are zoomed-in subfigures of **(a)** and **(c)**, respectively.

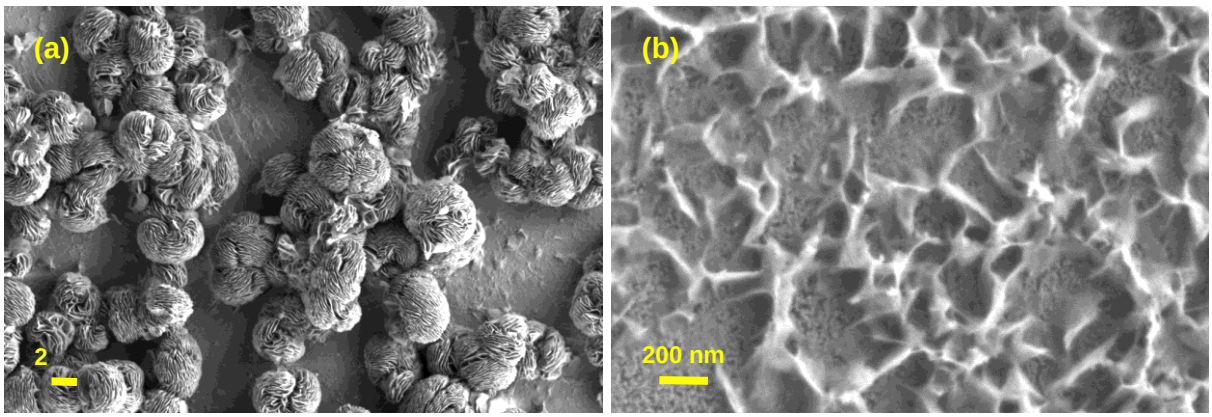

Figure 2: SEM images of ISG after 1 y in tests **(a)** S1-Blk-10.1, showing the precipitation of CSH-like phases, and **(b)** S1-Sat-10.1, showing minimal precipitation of phyllosilicates.

Time (d)	S1-Sat-1	S1-Blk-3	S1-Sat-3	S1-Blk-7	S1-Sat-7	S1-Sat-8	S1-Sat-9	S1-Blk-9.5	S1-Sat-9.5	S1-Sat-9.8	S1-Blk-10.1	S1-Sat-10.1	S1-Sat-10.3
0	$3.1 \cdot 10^{2}$	3.3	$3.0 \cdot 10^{2}$	2.2	$1.5 \cdot 10^{2}$	$1.8 \cdot 10^{2}$	$2.8 \cdot 10^{2}$	5.7	$7.4 \cdot 10^{2}$	$1.3 \cdot 10^{3}$	$2.4 \cdot 10^{1}$	$3.8 \cdot 10^{3}$	$1.2 \cdot 10^{4}$
1.2	$2.9 \cdot 10^{2}$	$8.4 \cdot 10^{1}$	$3.1 \cdot 10^{2}$	$1.7 \cdot 10^{1}$	$1.5 \cdot 10^{2}$	$1.5 \cdot 10^{2}$	$2.5 \cdot 10^{2}$	$2.0 \cdot 10^{1}$	$6.4 \cdot 10^{2}$	$1.2 \cdot 10^{3}$	$3.6 \cdot 10^{1}$	$3.4 \cdot 10^{3}$	$9.9 \cdot 10^{3}$
7.2	$3.1 \cdot 10^{2}$	$3.3 \cdot 10^{1}$	$3.2 \cdot 10^{2}$	$5.9 \cdot 10^{1}$	$1.4 \cdot 10^{2}$	$1.5 \cdot 10^{2}$	$2.8 \cdot 10^{2}$	$3.6 \cdot 10^{1}$	$6.3 \cdot 10^{2}$	$1.2 \cdot 10^{3}$	$6.7 \cdot 10^{1}$	$3.5 \cdot 10^{3}$	$1.1 \cdot 10^{4}$
14.2	$3.4 \cdot 10^{2}$	$4.6 \cdot 10^{1}$	$3.1 \cdot 10^{2}$	$6.3 \cdot 10^{1}$	$1.4 \cdot 10^{2}$	$1.5 \cdot 10^{2}$	$2.5 \cdot 10^{2}$	$4.2 \cdot 10^{1}$	$5.9 \cdot 10^{2}$	$1.2 \cdot 10^{3}$	$6.7 \cdot 10^{1}$	$3.4 \cdot 10^{3}$	$9.7 \cdot 10^{3}$
28.2	$4.9 \cdot 10^{2}$	$5.5 \cdot 10^{1}$	$3.2 \cdot 10^{2}$	$6.6 \cdot 10^{1}$	$1.4 \cdot 10^{2}$	$1.5 \cdot 10^{2}$	$2.5 \cdot 10^{2}$	$4.4 \cdot 10^{1}$	$5.5 \cdot 10^{2}$	$1.0 \cdot 10^{3}$	$7.5 \cdot 10^{1}$	$2.8 \cdot 10^{3}$	$1.0 \cdot 10^{4}$
91.1	$5.9 \cdot 10^{2}$	$9.3 \cdot 10^{1}$	$3.6 \cdot 10^{2}$	$7.6 \cdot 10^{1}$	$1.8 \cdot 10^{2}$	$1.6 \cdot 10^{2}$	$2.8 \cdot 10^{2}$	$6.2 \cdot 10^{1}$	NA	$1.6 \cdot 10^{3}$	$1.4 \cdot 10^{2}$	NA	$1.8 \cdot 10^{4}$
364.6	$5.6 \cdot 10^{2}$	$6.0 \cdot 10^{2}$	$9.5 \cdot 10^{2}$	$2.5 \cdot 10^{2}$	$3.3 \cdot 10^{2}$	$2.6 \cdot 10^{2}$	$4.7 \cdot 10^{2}$	$1.4 \cdot 10^{2}$	$8.4 \cdot 10^{2}$	$1.3 \cdot 10^{3}$	$5.1 \cdot 10^{2}$	$4.0 \cdot 10^{3}$	$1.2 \cdot 10^{4}$

Table 3: Silicon concentrations of the S1 test series, expressed in $g \cdot m^{-3}$ ($mg \cdot L^{-1}$) (NA: not analyzed).

Time (d)	S2-Blk-9.5	S2-Sat-9.5	S2-Blk-9.8	S2-Sat-9.8	S2-Blk-10.1	S2-Sat-10.1	S2-Blk-10.3	S2-Sat-10.3	S2-Blk-10.7	S2-Sat-10.7
0.0	4.3	$7.2 \cdot 10^{2}$	2.8	$1.8 \cdot 10^{3}$	2.1	$3.8 \cdot 10^{3}$	3.0	$1.1 \cdot 10^{4}$	6.8	$3.5 \cdot 10^{4}$
1.1	$1.9 \cdot 10^{1}$	$6.3 \cdot 10^{2}$	$1.0 \cdot 10^{2}$	$1.2 \cdot 10^{3}$	$1.5 \cdot 10^{2}$	$3.5 \cdot 10^{3}$	$1.1 \cdot 10^{2}$	$1.0 \cdot 10^{4}$	$1.8 \cdot 10^{2}$	$2.7 \cdot 10^{4}$
3.0	$2.1 \cdot 10^{1}$	$6.0 \cdot 10^{2}$	$1.2 \cdot 10^{2}$	$1.1 \cdot 10^{3}$	$1.6 \cdot 10^{2}$	$3.4 \cdot 10^{3}$	$1.2 \cdot 10^{2}$	$9.4 \cdot 10^{3}$	$2.0 \cdot 10^{2}$	$2.9 \cdot 10^{4}$
7.0	$1.9 \cdot 10^{1}$	$6.2 \cdot 10^{2}$	$1.5 \cdot 10^{2}$	$1.2 \cdot 10^{3}$	$1.6 \cdot 10^{2}$	$3.6 \cdot 10^{3}$	$1.3 \cdot 10^{2}$	$9.4 \cdot 10^{3}$	$2.3 \cdot 10^{2}$	$2.5 \cdot 10^{4}$
14.0	$1.9 \cdot 10^{1}$	$5.5 \cdot 10^{2}$	$1.9 \cdot 10^{2}$	$1.3 \cdot 10^{3}$	$1.5 \cdot 10^{2}$	$3.3 \cdot 10^{3}$	$1.2 \cdot 10^{2}$	$1.0 \cdot 10^{4}$	$1.9 \cdot 10^{2}$	$2.5 \cdot 10^{4}$
28.1	$1.9 \cdot 10^{1}$	$3.3 \cdot 10^{2}$	$1.4 \cdot 10^{2}$	$1.1 \cdot 10^{3}$	$1.4 \cdot 10^{2}$	$3.5 \cdot 10^{2}$	$1.7 \cdot 10^{2}$	$8.6 \cdot 10^{3}$	$2.2 \cdot 10^{2}$	$2.5 \cdot 10^{4}$
91.1	$1.2 \cdot 10^{1}$	$5.1 \cdot 10^{2}$	$1.9 \cdot 10^{2}$	$9.4 \cdot 10^{2}$	$1.9 \cdot 10^{2}$	$3.0 \cdot 10^{3}$	$2.0 \cdot 10^{2}$	$8.0 \cdot 10^{3}$	$2.2 \cdot 10^{2}$	$2.4 \cdot 10^{4}$
379.0	$3.6 \cdot 10^{1}$	$5.5 \cdot 10^{2}$	$2.2 \cdot 10^{2}$	$9.5 \cdot 10^{2}$	$3.2 \cdot 10^{2}$	$2.1 \cdot 10^{3}$	$3.5 \cdot 10^{2}$	$1.1 \cdot 10^{4}$	$5.2 \cdot 10^{2}$	$2.5 \cdot 10^{4}$

195 **Table 4:** Silicon concentrations of the S2 test series, expressed in $g \cdot m^{-3}$ ($mg \cdot L^{-1}$).

3.2. S2 test series: high *S*/*V* ratio

As in the S1 test series, the pHs in the S2 test series were maintained around the set values during the first 100 d (Figure A.2). However, the pH decreased significantly between 100 d and 1 y: by accident this variation was not compensated by alkaline additions. The evolution of the silicon concentration is summarized in Table 4, and the complete results of the solution analyses are presented in Appendix D. In the “S2-Blk” tests (Figure 3.a, Figure 4.a, Figure 5.a), the equivalent altered thicknesses for experiments conducted at all pHs are similar during the first 100 d, and increase slightly with decreasing pH from 10.7 (S2-Blk-10.7) and 9.5 (S2-Blk-9.5). Between 100 d and 1 y, only results from the experiment conducted at the highest pH ($pH_{90\,°C}$ = 10.7) deviates from this trend, as the samples are altered faster. The higher altered equivalent thicknesses in this test correlate with the precipitation of secondary phases, which could be identified as calcium aluminum silicate hydrates by XRD.

In the “S2-Sat” test series (Figure 4.b, Figure 5.b), larger amounts of secondary phases can be identified: oxyhydroxides, silicates, carbonates, and zeolites. The higher the pH, the greater the amount of precipitated crystalline phases after 1 y of leaching will be. These greater amounts of secondary phases result in greater equivalent thicknesses of altered glass. In detail (Figure 5):

- no diffraction peaks are observed at $pH_{90\,°C}$ <10.1;
- at $pH_{90\,°C}$ = 10.1 (S2-Sat-10.1): potassium calcium silicate hydrate (PDF 04-012-5493, $K_2Ca_2Si_8O_{19}\cdot(H_2O_4)$) and potassium sodium silicate (04-014-8491, $K_4Na_2Si_6O_{15}$) can be identified;
- at $pH_{90\,°C}$ = 10.3 (S2-Sat-10.3): potassium calcium silicate hydrate (04-012-5493), potassium hydrogen carbonate (04-013-5503, $HK(CO_3)$), sodium silicate (00-018-1241, $Na_2Si_2O_5$), and leucite (00-038-1423, $KAlSi_2O_6$) are present;
- at $pH_{90\,°C}$ = 10.7 (S2-Sat-10.7): potassium calcium silicate hydrate (04-012-5493), hydrogen potassium sodium carbonate hydrate (04-010-8201, $C_2H_5K_2NaO_8$), shlykovite (00-061-0758, $KCa(Si_4O_9(OH))\cdot 3H_2O$), phillipsite-K (00-034-0542), and leucite (00-038-

1423) are observed. In addition, the XRD patterns exhibit a broad reflection around 2θ = 30°, which is characteristic of CSH [45, 46].

Figure 3.b shows that the altered thicknesses are higher in the test at $pH_{90°C}$ = 10.7. For the other pHs, glass dissolution decreases during the first tens of days whatever the pH, before a further increase occurs for $pH_{90°C}$ = 10.1 and 10.3 (Appendix B). The higher the pH, the faster and earlier is this increase.

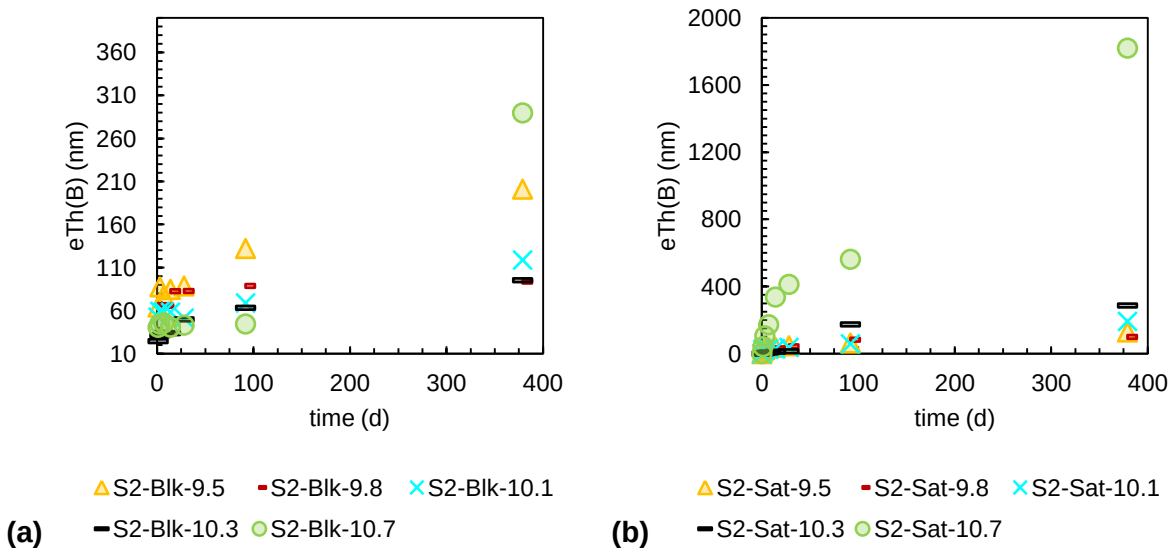

Figure 3: Evolution of the equivalent thickness of altered glass calculated from the boron concentration, eTh(B), for the **(a)** S2-Blk and **(b)** S2-Sat test series with an *S/V* ratio of 10 000 m^{-1}. Zoomed-in subfigures are presented in Appendix B.

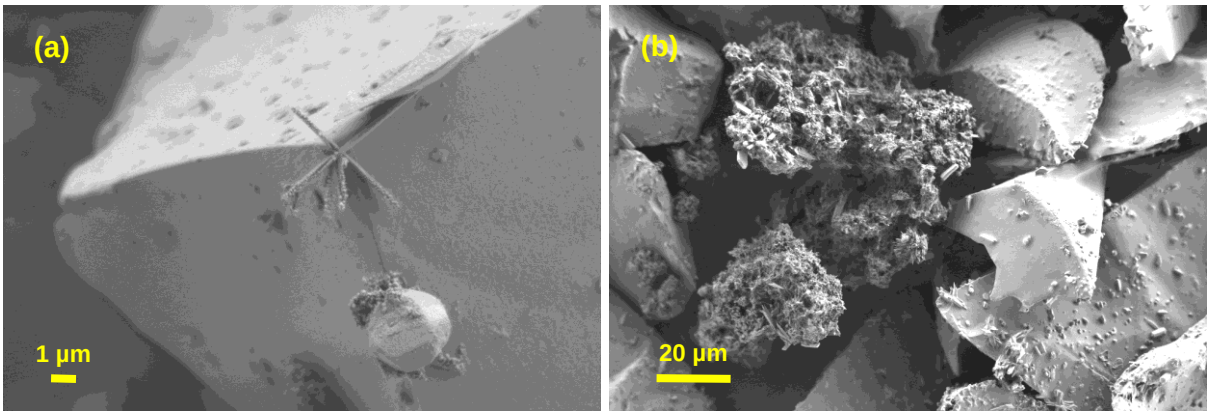

Figure 4: Secondary electron SEM images after 1 y for tests **(a)** S2-Blk-10.3 and **(b)** S2-Sat-10.3.

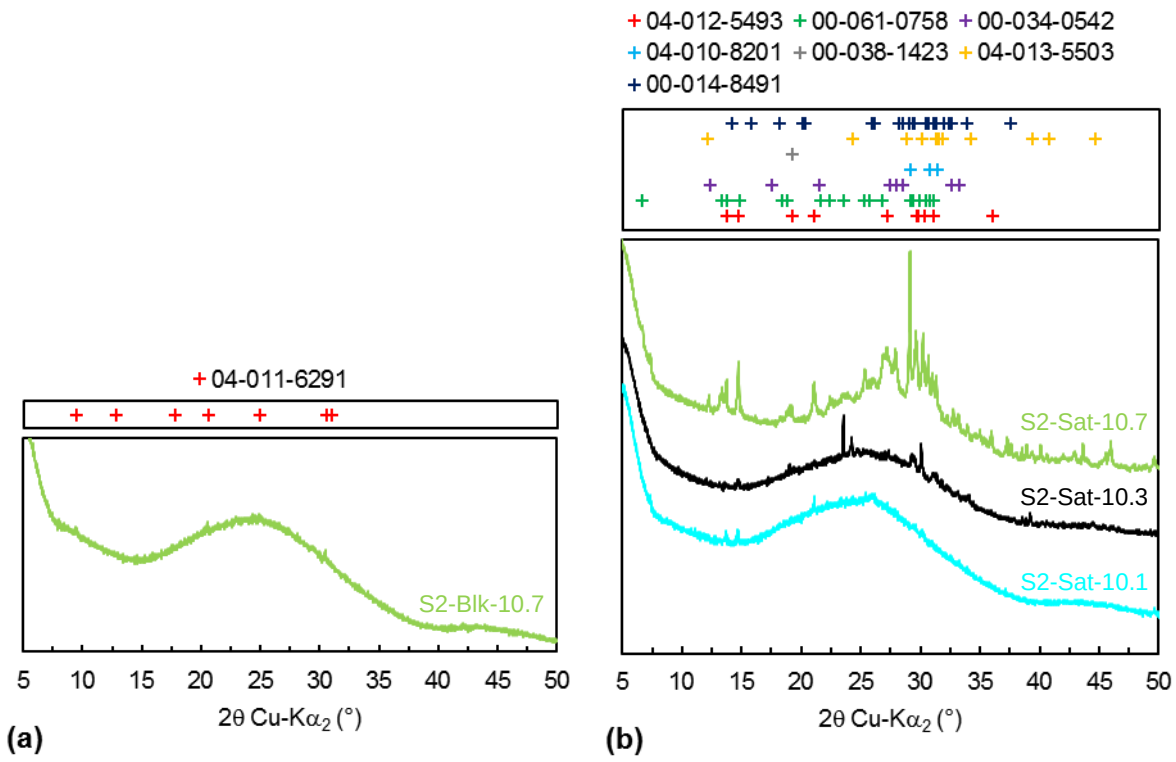

Figure 5: X-ray diffraction patterns for the S2 **(a)** "Blk" and **(b)** "Sat" test series. The positions of the major peaks ($I \geq 0.3 \times I_{max}$) in reference diffractograms (PDF-4+ 2018 RDB, database 4.1801) corresponding to the identified phases are indicated: K-Ca-Si oxyhydroxide (PDF 04-012-5493), shlykovite (PDF 00-061-0758), phillipsite-K (PDF 00-034-0542), Na-K carbonate (PDF 04-010-8201), leucite (PDF 00-038-1423), K carbonate (PDF 04-013-5503), K-Na-Si oxide (PDF 04-014-8491), and Ca-Al-Si hydrate (PDF 04-011-6291).

4. Discussion

A "low" *S*/*V* ratio was selected for the S1 test series to maintain a large difference in the silica concentration between the "S1-Sat" test series (aqueous silica-containing solutions) and the "S1-Blk" test series (solutions without silica) for as long as possible. However, the results show that this experimental design did not allow for quantification of the glass alteration in strongly alkaline solutions because of the dilution of the samples (necessitated by the high silica concentrations) required for ICP-OES analysis (e.g., dilution factor > 200 at $pH_{90\,°C}$ = 10.3). To circumvent this shortcoming, the S2 test series was conducted with a higher *S*/*V* ratio and focused on alkaline pHs. However, it was more difficult to highlight the effect of the initial solution under these conditions because the solutions rapidly reached saturation owing to the greater surface area of the glass. As an example, assuming no retention of silica in the gel nor precipitation of secondary silicate phases, at $pH_{90\,°C}$ = 9.8, it is necessary to dissolve 35 µm of glass to reach

saturation with respect to amorphous silica at S/V = 60 cm^{-1}, and only 0.2 µm at S/V = 10 000 cm^{-1}. Both the S1 and S2 test series will be considered in the following discussion.

In the S1 test series and at $pH_{90\,°C}$ = 1 (S1-Sat-1), an initial dissolution rate of 3.2 $g \cdot m^{-2} \cdot d^{-1}$ is calculated between 0 and 7 days by linear regression from boron release (despite the beginning of inflection of the alteration rate). This value can be compared to that acquired at 90°C and $pH_{90\,°C}$ = 1.5 by Pérez, *et al.* [47] of ≈ 2.5 $g \cdot m^{-2} \cdot d^{-1}$. The fact that these two values are close, added to the comparison in the equivalent thickness of altered glass between the "S1-Blk" and "S1-Sat" tests (Figure 6.a and Figure C.1) shows that the effect of aqueous silica on the glass dissolution is negligible at $pH_{90\,°C} \leq 3$. However, the effect of aqueous silica becomes more significant at $pH_{90\,°C}$ = 7: the equivalent thickness of the altered glass at the end of the S1-Blk-7 test is 1.5 to 3 times greater than that for the S1-Sat-7 test (Figure C.1.b). This difference increases significantly with the pH, from a factor of ≈ 35 at $pH_{90\,°C}$ = 9.5 (S1-Blk-9.5 vs. S1-Sat-9.5) to a factor of ≈ 60 at $pH_{90\,°C}$ = 10.1 (S1-Blk-10.1 vs. S1-Sat-10.1). At $pH_{90\,°C}$ = 9.5 and 10.1 in the S1 test series, the gap due to the initial presence of aqueous silica should likely be even greater before 1 y. Indeed, the silicon concentrations in solution due to the glass dissolution in the S1-Blk-9.5 and S1-Blk-10.1 tests end up being significantly high after 1 y ($1.4 \cdot 10^2$ $mg \cdot L^{-1}$ and $5.1 \cdot 10^2$ $mg \cdot L^{-1}$ respectively, Table 3). Therefore, it is clear from the S1 test series that aqueous silica causes an increase in glass durability above a threshold of $pH_{90\,°C} \approx 7$, and this effect increases with pH, at least up to $pH_{90\,°C} \approx 10.1$, with a low S/V ratio of 60 m^{-1}. This beneficial effect on the glass durability can be interpreted as the rapid formation of a passivating layer in the silica-rich solutions of the "S1-Sat" test series [11], while partial dissolution of the glass in the "S1-Blk" tests is required to reach saturation. An increase in glass durability with the addition of silica in solution was also observed for SON68 glass at 90 °C and pH = 9 [20]. Note that by focusing only on silica, it is possible that the rate drop tied to the affinity effect is lower than that expected with a solution saturated with all the glass constituents. This verification is difficult and requires the use of isotopes to monitor the glass dissolution rate.

Unexpectedly, the results of the S1 test series show that aqueous silica seems to have no direct nor indirect effect on the glass alteration at acidic pH. This could be for several reasons: (i) the rate was calculated from the release of B, and it can be hypothesized that B is preferentially leached out in acidic pH along with alkalis, the release of which from glass is known to be driven by ion-exchange [48-51]; or (ii) a passivating gel cannot form because the condensation reactions are slower in acidic pH than in basic pH [34]. At this stage, it is not possible to decide between these two hypotheses.

On the one hand, the first hypothesis is supported by the observation that in the S1-Blk-3 test B and Na are released congruently, following a square root-dependent time law until total alteration of the glass (Figure 7.a). Thus, it is plausible that ion-exchange is responsible for the release of Na and that the penetration of hydronium ions into the glass also drives the hydrolysis of B. At $pH_{90\,°C}$ = 3 (S1-Blk-3), Si dissolves approximately 20 times slower than B and Na. This preferential release of B and Na relative to Si suggests that a thick Si-rich surface layer will remain. The observed preferential leaching of B and Na relative to Si in acidic conditions also explains why the initial Si concentration in solution is not a determinant parameter in acidic systems. In contrast, at $pH_{90\,°C}$ = 10.1 (S1-Blk-10.1), B, Na, and Si dissolve at almost the same rate (Figure 7.b). These results suggest that in the $pH_{90\,°C}$ range of 7–9.5, the release of weakly bonded elements such as Na and B is controlled by hydrolysis-condensation reaction within the aluminosilicate network.

On the other hand, the second hypothesis stating that a passivating gel cannot form at acidic pH is similar to the one suggested by Daval*, et al.* [52] to account for the passivating ability of Si-rich layers developed on slow-dissolving wollastonite cleavage planes as opposed to fast-dissolving cleavage planes. More generally, the non-passivating behavior of silica layers developed in acidic solutions has previously been demonstrated by the mineralogical community for a series of Fe-free silicate minerals altered at acidic pH, including wollastonite [53], feldspars [54-57] and forsterite [58]. In particular, Wild*, et al.* [56] demonstrated that the Si-rich layers formed on labradorite switched from non-passivating at pH ≤ 2.5 to passivating at pH > 2.5, indicating that

the pH value for passivation is lower for feldspars than for ISG. This suggests that there might be a strong coupling between the intrinsic dissolution rate of the parent phase (which increases with decreasing pH in the acidic pH range) and the rate of the silica layer condensation/polymerization (which decreases with decreasing pH in the acidic pH range).

The S2 test series with the higher *S*/*V* ratio of 10 000 m^{-1} can provide valuable new insights through comparison with the first series. Indeed, at $pH_{90\,°C}$ = 9.8 and *S*/*V* = 10 000 m^{-1}, i.e., the pH at which it has been shown that the presence of aqueous silica causes a dramatic decrease in the glass alteration, the altered glass fraction is the same in the S2-Blk-9.8 and S2-Sat-9.8 tests after a year, irrespective of the initial aqueous silica concentration of the solution (Figure 6.b and Figure C2.b). This trend is different at $pH_{90\,°C}$ = 10.1, 10.3, and 10.7, where the glass is significantly more altered in the “S2-Sat” silica-rich solutions. This can be interpreted as a destabilization of the passivating gel whose formation was favored by the initial presence of aqueous silica. This destabilization could be linked to the precipitation of Si-rich secondary phases: C(A)SH, zeolites, carbonates, and poorly crystallized hydrated and anyhdrous silicates. Of these secondary phases, C(A)SH and zeolites are already known to be at the origin of the so-called “resumption of alteration” phenomenon that leads to an acceleration of the glass alteration rate [59]. The formation of a passivating gel before the formation of zeolites has been documented [38], and its destabilization due to their precipitation is consistent with the experimental results reported by Fournier*, et al.* [7] and the associated modeling [60]. Table 3 shows that the precipitation of these Si-bearing minerals does not necessarily go with a decrease in the silicon concentration. This can be explained by a Si/*i* ratio of the phases (with *i* the chemical element limiting their precipitation) lower than the Si/*i* ratio of the glass. This result is well known when zeolites precipitate during resumptions of alteration of glasses [7, 59, 61, 62].

For the three most alkaline pHs in this second test series ($pH_{90\,°C}$ = 10.1, 10.3, and 10.7), a significant difference is observed between the silica concentrations reached in the “S2-Blk” tests (≈ 300 to 500 $g \cdot m^{-3}$) and those in the pre-saturated solution “S2-Sat” tests ($2 \cdot 10^3$ to $2.5 \cdot 10^4$ $g \cdot m^{-}$

^{3}) (Figure 6.c). This difference increases with the pH. At $pH_{90\,°C}$ = 9.5 (S2-Blk-9.5 vs. S2-Sat-9.5), the difference in the silica concentrations is small, and it is expected that this difference would decrease further at longer times. Indeed, it was demonstrated in a 14-year-long experiment [63] that a solution at this pH will eventually achieve equilibrium with amorphous silica. This was possible because no secondary phases precipitated at this pH. Here, because silicate minerals precipitate above $pH_{90\,°C}$ = 9.5, they partly control the solution composition. Studies conducted at high pH have shown that the precipitation of silicate minerals such as CSH and zeolites is not instantaneous; there is an induction period during which the glass dissolves slowly before alteration resumes [7, 59, 61]. During this so-called “plateau regime,” the solution composition, and possibly the transport of reactive species toward the pristine glass surface, are controlled by various amorphous materials, whose composition, structure, and diffusion properties are poorly understood [16, 64, 65]. The mechanisms for the formation of these materials are pH-dependent, although the average composition of the alteration layer (gel and secondary phases) deduced from the elemental concentrations in solution varies little regardless of the pH: $SiAl_{0.2\pm0.1}Ca_{0.1\pm0.1}Zr_{0.05\pm0.03}$.

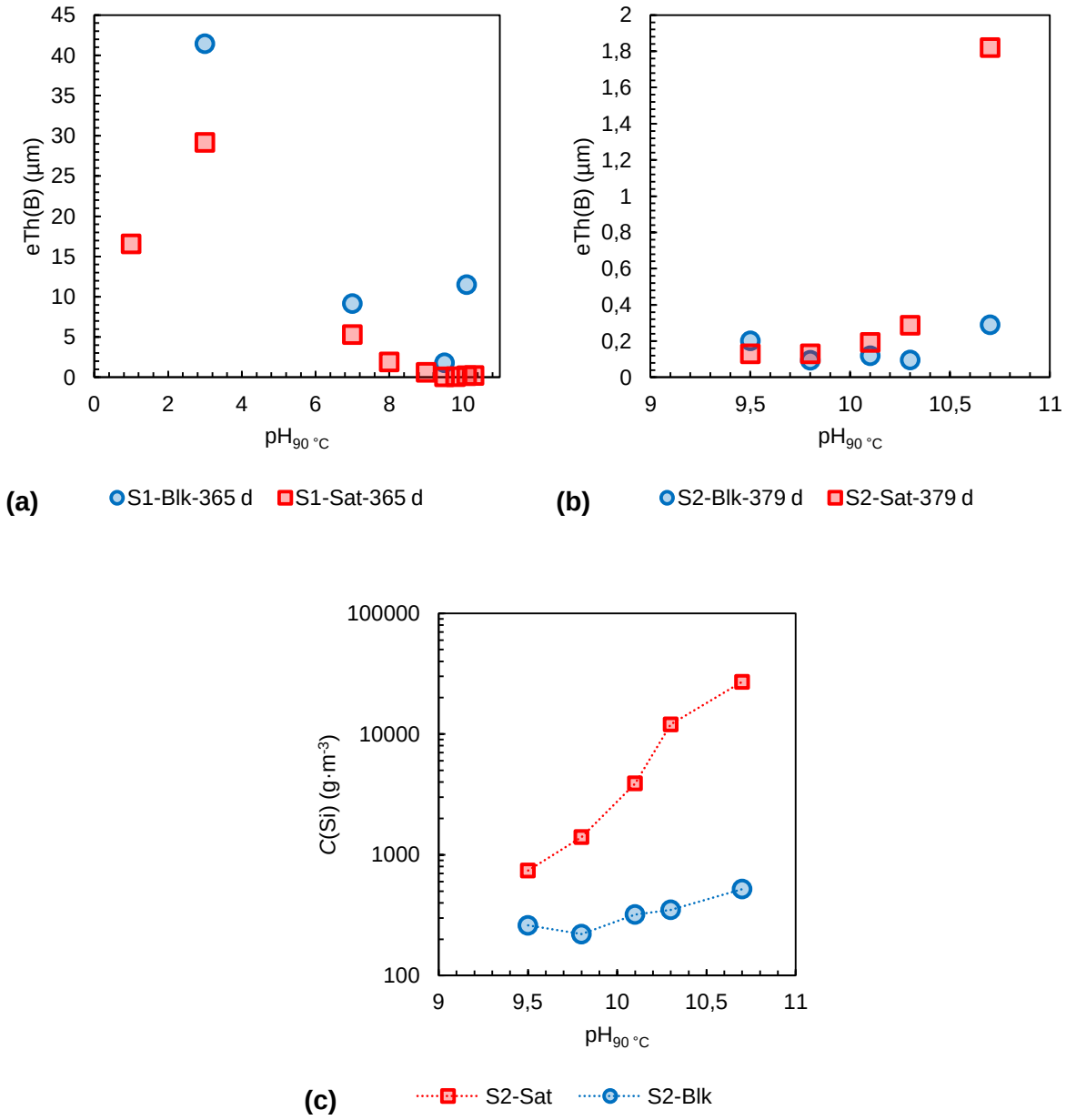

Figure 6: Comparison of the equivalent thickness of altered glass calculated from the boron concentrations, eTh(B), at the last sampling time (≈ 1 y) at various pH for the **(a)** S1 test series (S/V = 60 m^{-1}) and **(b)** S2 test series (S/V = 10 000 m^{-1}). **(c)** Comparison of the silicon concentrations, C(Si), reached at the end of the experiment (379 d) at various pH for the S2 test series.

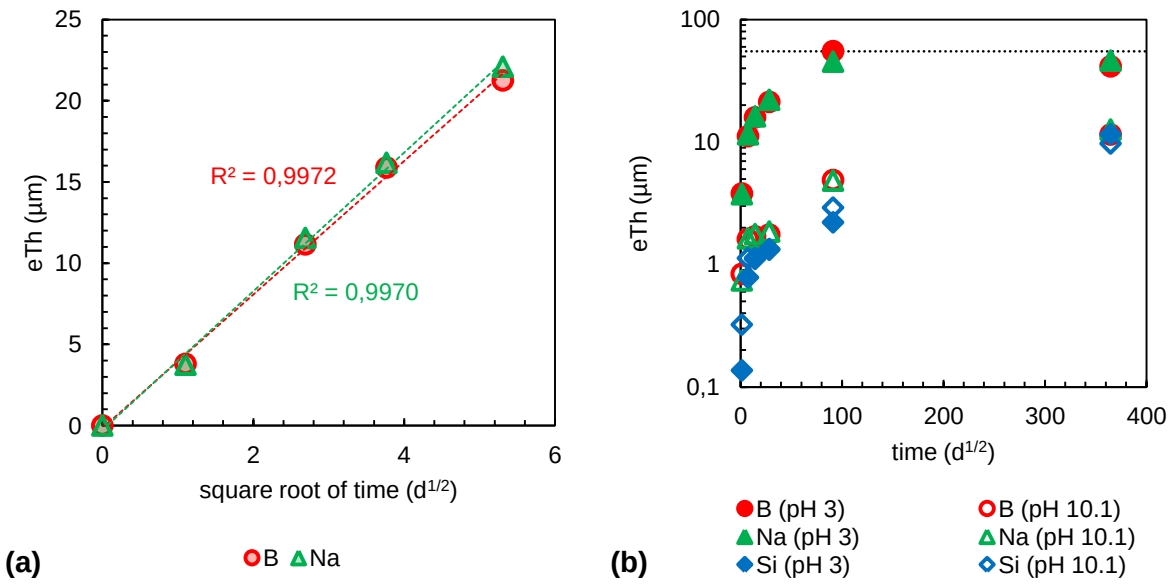

Figure 7: (a) Evolution of the equivalent thickness of altered glass, eTh, calculated from boron and sodium concentrations as a function of the square root of the time during the first month for the S1-Blk-3 test. **(b)** Comparison of the evolution of B, Na, and Si eTh for the S1-Blk-3 (plain symbols) and S1-Blk-10.1 (open symbols) tests. The dotted line represents the total alteration of the glass (%AG = 100).

5. Conclusions

For a silica concentration equal to that reached at saturation with amorphous silica, the experimental work reported in this study shows a negligible effect of aqueous silica on the glass dissolution rate (measured from B release) at acidic pH and a marked effect above $pH_{90\,°C}$ = 7 with a low *S*/*V* ratio of 60 m^{-1}, thus ensuring better chemical durability of the glass. Thus, pH-induced changes in solution chemistry shift the equilibria. At a higher *S*/*V* ratio of 10 000 m^{-1} and at $pH_{90\,°C} \geq 9.5$, the aqueous silica decreases the glass durability due to the formation of secondary phases (Figure 8). Most of the phases identified are hydroxides, which are likely precursors of better-crystalized phases formed by Ostwald ripening.

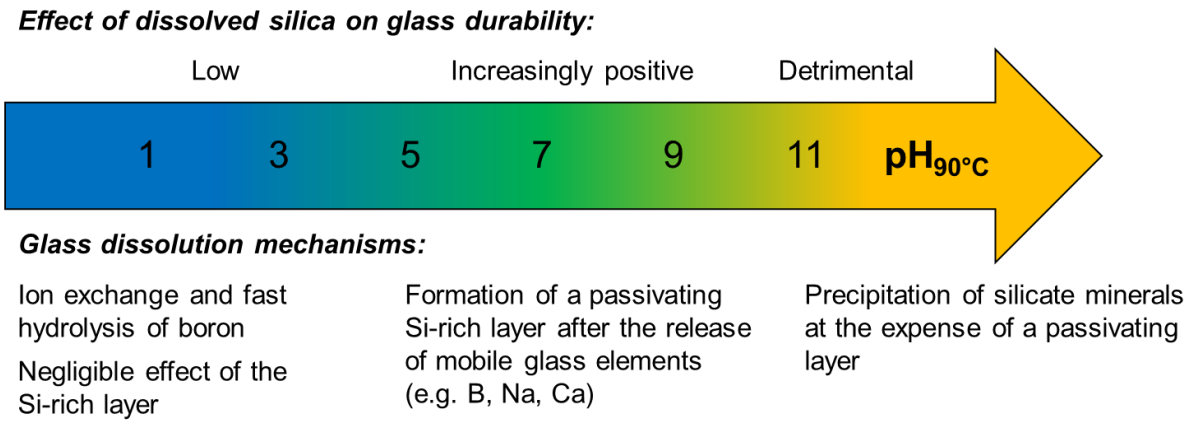

Figure 8: Diagram summarizing the effects of dissolved silica on the glass dissolution mechanisms as a function of pH.

Acknowledgements

This research was supported by ANDRA. The authors are grateful to Jean-Pierre Mestre for SEM analysis, Géraldine Parisot and the laboratory CEA/DEN/DMRC/SA2I/LMAC for ICP-OES analysis.

Data availability statement

The authors declare that the data supporting the findings of this study are available within the article and its appendixes, and from the corresponding author upon reasonable request.

References

[1] B. Grambow, Nuclear waste glasses; how durable?, Elements 2(6) (2006) 357-364.
[2] C. Fillet, I. Ribet, S. Gin, S. Peuget, E. Vernaz, Long term behaviour of French R7T7 glass: a short review, Glass Technol. 49(6) (2008) 302-306.
[3] E. Curti, J.L. Crovisier, G. Morvan, A.M. Karpoff, Long-term corrosion of two nuclear waste reference glasses (MW and SON68): A kinetic and mineral alteration study, Appl. Geochem. 21(7) (2006) 1152-1168.
[4] B.M.J. Thien, N. Godon, A. Ballestero, S. Gin, A. Ayral, The dual effect of Mg on the long-term alteration rate of AVM nuclear waste glasses, J. Nucl. Mater. 427(1-3) (2012) 297-310.
[5] H. Aréna, N. Godon, D. Rébiscoul, R. Podor, E. Garcès, M. Cabie, J.P. Mestre, Impact of Zn, Mg, Ni and Co elements on glass alteration: Additive effects, J. Nucl. Mater. 470 (2016) 55-67.

[6] H. Aréna, N. Godon, D. Rébiscoul, P. Frugier, R. Podor, E. Garcès, M. Cabie, J.P. Mestre, Impact of iron and magnesium on glass alteration: Characterization of the secondary phases and determination of their solubility constants, Appl. Geochem. 82 (2017) 119-133.
[7] M. Fournier, S. Gin, P. Frugier, S. Mercado-Depierre, Contribution of zeolite seeded experiments to the understanding of resumption of glass alteration, npj Mater. Degrad. 1 (2017) 17.
[8] E. Burger, D. Rebiscoul, F. Bruguier, M. Jublot, J.E. Lartigue, S. Gin, Impact of iron on nuclear glass alteration in geological repository conditions: A multiscale approach, Appl. Geochem. 31 (2013) 159-170.
[9] B. Fleury, N. Godon, A. Ayral, S. Gin, SON68 glass dissolution driven by magnesium silicate precipitation, J. Nucl. Mater. 442(1) (2013) 17-28.
[10] N. Valle, A. Verney-Carron, J. Sterpenich, G. Libourel, E. Deloule, P. Jollivet, Elemental and isotopic (^{29}Si and ^{18}O) tracing of glass alteration mechanisms, Geochim. Cosmochim. Acta 74(12) (2010) 3412-3431.
[11] S. Gin, P. Jollivet, M. Fournier, F. Angeli, P. Frugier, T. Charpentier, Origin and consequences of silicate glass passivation by surface layers, Nat. Commun. 6 (2015) 6360.
[12] S. Gin, M. Collin, P. Jollivet, M. Fournier, Y. Minet, L. Dupuy, T. Mahadevan, S. Kerisit, J. Du, Dynamics of self-reorganization explains passivation of silicate glasses, Nat. Commun. 9(1) (2018) 2169.
[13] L. Neill, S. Gin, T. Ducasse, T. De Echave, M. Fournier, P. Jollivet, A. Gourgiotis, N.A. Wall, Various effects of magnetite on international simple glass (ISG) dissolution: implications for the long-term durability of nuclear glasses, npj Mater. Degrad. 1(1) (2017) 1.
[14] T. De Echave, M. Tribet, P. Jollivet, C. Marques, S. Gin, C. Jégou, Effect of clayey groundwater on the dissolution rate of SON68 simulated nuclear waste glass at 70 °C, J. Nucl. Mater. 503 (2018) 279-289.
[15] P. Frugier, S. Gin, Y. Minet, T. Chave, B. Bonin, N. Godon, J.E. Lartigue, P. Jollivet, A. Ayral, L. De Windt, G. Santarini, SON68 nuclear glass dissolution kinetics: Current state of knowledge and basis of the new GRAAL model, J. Nucl. Mater. 380(1-3) (2008) 8-21.
[16] P. Frugier, Y. Minet, N. Rajmohan, N. Godon, S. Gin, GRAAL, a model for glass corrosion, npj Mater. Degrad. In Press (2018).
[17] P. Van Iseghem, M. Aertsens, S. Gin, D. Deneele, B. Grambow, D. Strachan, P. McGrail, G. Wicks, GLAMOR - Or how we achieved a common understanding on the decrease of glass dissolution kinetics, Ceram. Trans. 207(s) (2009) 115-126.
[18] J.P. Icenhower, B.P. McGrail, W.J. Shaw, E.M. Pierce, P. Nachimuthu, D.K. Shuh, E.A. Rodriguez, J.L. Steele, Experimentally determined dissolution kinetics of Na-rich borosilicate glass at far from equilibrium conditions: Implications for Transition State Theory, Geochim. Cosmochim. Acta 72(12) (2008) 2767-2788.
[19] J. Neeway, A. Abdelouas, B. Grambow, S. Schumacher, Dissolution mechanism of the SON68 reference nuclear waste glass: New data in dynamic system in silica saturation conditions, J. Nucl. Mater. 415(1) (2011) 31-37.
[20] S. Gin, P. Frugier, P. Jollivet, F. Bruguier, E. Curti, New insight into the residual rate of borosilicate glasses: Effect of S/V and glass composition, Int. J. Appl. Glass Sci. 4(4) (2013) 371-382.
[21] S. Gin, P. Frugier, SON68 glass dissolution kinetics at high reaction progress: Experimental evidence of the residual rate, Mater. Res. Soc. Symp. Proc. 757 (2003) II5.9.
[22] T. Advocat, J.L. Chouchan, J.L. Crovisier, C. Guy, V. Daux, C. Jegou, S. Gin, E. Vernaz, Borosilicate nuclear waste glass alteration kinetics: Chemical inhibition and affinity control, Mater. Res. Soc. Symp. Proc. 506 (1998) 63-70.
[23] S. Gin, L. Neill, M. Fournier, P. Frugier, T. Ducasse, M. Tribet, A. Abdelouas, B. Parruzot, J. Neeway, N. Wall, The controversial role of inter-diffusion in glass alteration, Chem. Geol. 440 (2016) 115-123.
[24] P. Jollivet, S. Gin, S. Schumacher, Forward dissolution rate of silicate glasses of nuclear interest in clay-equilibrated groundwater, Chem. Geol. 330-331 (2012) 207-217.
[25] S. Mercado-Depierre, F. Angeli, F. Frizon, S. Gin, Antagonist effects of calcium on borosilicate glass alteration, J. Nucl. Mater. 441(1) (2013) 402-410.

[26] T. Chave, P. Frugier, S. Gin, A. Ayral, Glass-water interphase reactivity with calcium rich solutions, Geochim. Cosmochim. Acta 75(15) (2011) 4125-4139.
[27] P. Jollivet, P. Frugier, G. Parisot, J.P. Mestre, E. Brackx, S. Gin, S. Schumacher, Effect of clayey groundwater on the dissolution rate of the simulated nuclear waste glass SON68, J. Nucl. Mater. 420(1-3) (2012) 508-518.
[28] H. Aréna, D. Rébiscoul, R. Podor, E. Garcès, M. Cabie, J.P. Mestre, N. Godon, Impact of Fe, Mg and Ca elements on glass alteration: Interconnected processes, Geochim. Cosmochim. Acta 239 (2018) 420-445.
[29] N. Cassingham, C.L. Corkhill, D.J. Backhouse, R.J. Hand, J.V. Ryan, J.D. Vienna, N.C. Hyatt, The initial dissolution rates of simulated UK Magnox–ThORP blend nuclear waste glass as a function of pH, temperature and waste loading, Mineral. Mag. 79(6) (2015) 1529-1542.
[30] C.L. Corkhill, A.J. Fisher, D.M. Strachan, R.J. Hand, N.C. Hyatt, Corrigendum to “The dissolution rates of simulated UK Magnox – ThORP blend nuclear waste glass as a function of pH, temperature and waste loading” [Miner. Mag. 79, (2015) 1529–1542], Mineral. Mag. 82(4) (2018) 939-942.
[31] C.L. Corkhill, N.J. Cassingham, P.G. Heath, N.C. Hyatt, Dissolution of UK high-level waste glass under simulated hyperalkaline conditions of a colocated geological disposal facility, Int. J. Appl. Glass Sci. 4(4) (2013) 341-356.
[32] B. Craeye, G. De Schutter, H. Van Humbeeck, A. Van Cotthem, Concrete containers for containment of vitrified high-level radioactive waste: The Belgian approach, CRC Press-Taylor & Francis Group, Boca Raton, 2009.
[33] S. Gin, A. Abdelouas, L.J. Criscenti, W.L. Ebert, K. Ferrand, T. Geisler, M.T. Harrison, Y. Inagaki, S. Mitsui, K.T. Mueller, J.C. Marra, C.G. Pantano, E.M. Pierce, J.V. Ryan, J.M. Schofield, C.I. Steefel, J.D. Vienna, An international initiative on long-term behavior of high-level nuclear waste glass, Mater. Today 16(6) (2013) 243-248.
[34] R.K. Iler, The Chemistry of Silica: Solubility, Polymerization, Colloid and Surface Properties, and Biochemistry of Silica, John Wiley & Sons Inc.1979.
[35] S. Gin, P. Jollivet, G. Barba Rossa, M. Tribet, S. Mougnaud, M. Collin, M. Fournier, E. Cadel, M. Cabie, L. Dupuy, Atom-Probe Tomography, TEM and ToF-SIMS study of borosilicate glass alteration rim: A multiscale approach to investigating rate-limiting mechanisms, Geochim. Cosmochim. Acta 202 (2017) 57-76.
[36] M. Collin, M. Fournier, P. Frugier, T. Charpentier, M. Moskura, L. Deng, M. Ren, J. Du, S. Gin, Structure of International Simple Glass and properties of passivating layer formed in circumneutral pH conditions, npj Mater. Degrad. 2(1) (2018) 4.
[37] D. Ngo, H. Liu, N. Sheth, R. Lopez-Hallman, N.J. Podraza, M. Collin, S. Gin, S.H. Kim, Spectroscopic ellipsometry study of thickness and porosity of the alteration layer formed on international simple glass surface in aqueous corrosion conditions, npj Mater. Degrad. 2(1) (2018) 20.
[38] S. Gin, P. Jollivet, M. Fournier, C. Berthon, Z. Wang, A. Mitroshkov, Z. Zhu, J.V. Ryan, The fate of silicon during glass corrosion under alkaline conditions: A mechanistic and kinetic study with the International Simple Glass, Geochim. Cosmochim. Acta 151 (2015) 68-85.
[39] M. Fournier, A. Ull, E. Nicoleau, Y. Inagaki, M. Odorico, P. Frugier, S. Gin, Glass dissolution rate measurement and calculation revisited, J. Nucl. Mater. 476 (2016) 140-154.
[40] J. van der Lee, L. De Windt, V. Lagneau, P. Goblet, Module-oriented modeling of reactive transport with HYTEC, Comput. Geosci. 29(3) (2003) 265-275.
[41] ASTM International, Standard test method for silica in water, ASTM Standard S859, West Conshohocken, PA, United-States, 2010.
[42] S. Depierre, Etude des mécanismes d'altération du verre par des eaux cimentaires, PhD thesis of Université Montpellier 2, France, 2012.
[43] B. Thien, N. Godon, F. Hubert, F. Angéli, S. Gin, A. Ayral, Structural identification of a trioctahedral smectite formed by the aqueous alteration of a nuclear glass, Appl. Clay Sci. 49(3) (2010) 135-141.
[44] C. Zhu, D.R. Veblen, A.E. Blum, S.J. Chipera, Naturally weathered feldspar surfaces in the Navajo Sandstone aquifer, Black Mesa, Arizona: Electron microscopic characterization, Geochim. Cosmochim. Acta 70(18) (2006) 4600-4616.

[45] J.R. Houston, R.S. Maxwell, S.A. Carroll, Transformation of meta-stable calcium silicate hydrates to tobermorite: reaction kinetics and molecular structure from XRD and NMR spectroscopy, Geochem. Trans. 10 (2009).
[46] J.M. Fernández, A. Duran, I. Navarro-Blasco, J. Lanas, R. Sirera, J.I. Alvarez, Influence of nanosilica and a polycarboxylate ether superplasticizer on the performance of lime mortars, Cem. Concr. Res. 43 (2013) 12-24.
[47] A. Pérez, R. Saint-Lys, D. Lemarchand, M. Vital, D. Daval, M. Fournier, S. Gin, Etude de l'influence de la structure sur les mécanismes et cinétiques de dissolution d'une phase alumino silicatée. Etude de la stabilité du réseau vitreux en fonction du pH en milieu saturée en silice, Report, Contrat de collaboration de recherche N°069332 (Ref. CNRS : 138253), LHyGeS, CNRS, Université de Strasbourg, CEA, 2018.
[48] S. Mitsui, R. Aoki, Effect of a siliceous additive on aqueous alteration of waste glass with engineered barrier materials, J. Nucl. Mater. 298(1-2) (2001) 184-191.
[49] K. Ferrand, A. Abdelouas, B. Grambow, Water diffusion in the simulated French nuclear waste SON 68 contacting silica rich solutions: Experimental and modeling, J. Nucl. Mater. 355 (2006) 54-67.
[50] M.I. Ojovan, A. Pankov, W.E. Lee, The ion exchange phase in corrosion of nuclear waste glasses, J. Nucl. Mater. 358(1) (2006) 57-68.
[51] B.C. Bunker, Molecular mechanisms for corrosion of silica and silicate glasses, J. Non-Cryst. Solids 179 (1994) 300-308.
[52] D. Daval, S. Bernard, L. Rémusat, B. Wild, F. Guyot, J.S. Micha, F. Rieutord, V. Magnin, A. Fernandez-Martinez, Dynamics of altered surface layer formation on dissolving silicates, Geochim. Cosmochim. Acta 209 (2017) 51-69.
[53] D. Daval, I. Martinez, J.-M. Guigner, R. Hellmann, J. Corvisier, N. Findling, C. Dominici, B. Goffé, F. Guyot, Mechanism of wollastonite carbonation deduced from micro- to nanometer length scale observations, Am. Mineral. 94(11-12) (2009) 1707-1726.
[54] G. Jordan, S.R. Higgins, C.M. Eggleston, S.M. Swapp, D.E. Janney, K.G. Knauss, Acidic dissolution of plagioclase: in-situ observations by hydrothermal atomic force microscopy, Geochim. Cosmochim. Acta 63(19) (1999) 3183-3191.
[55] R. Hellmann, J.M. Penisson, R.L. Hervig, J.H. Thomassin, M.F. Abrioux, An EFTEM/HRTEM high-resolution study of the near surface of labradorite feldspar altered at acid pH: evidence for interfacial dissolution-reprecipitation, Phys. Chem. Miner. 30(4) (2003) 192-197.
[56] B. Wild, D. Daval, F. Guyot, K.G. Knauss, M. Pollet-Villard, G. Imfeld, pH-dependent control of feldspar dissolution rate by altered surface layers, Chem. Geol. 442 (2016) 148-159.
[57] A. Pérez, D. Daval, M. Fournier, M. Vital, J.-M. Delaye, S. Gin, Comparing the reactivity of glasses with their crystalline equivalents: the case study of plagioclase feldspar, Geochim. Cosmochim. Acta (2019).
[58] G.D. Saldi, D. Daval, G. Morvan, K.G. Knauss, The role of Fe and redox conditions in olivine carbonation rates: An experimental study of the rate limiting reactions at 90 and 150°C in open and closed systems, Geochim. Cosmochim. Acta 118 (2013) 157-183.
[59] M. Fournier, S. Gin, P. Frugier, Resumption of nuclear glass alteration: State of the art, J. Nucl. Mater. 448(1-3) (2014) 348-363.
[60] M. Fournier, P. Frugier, S. Gin, Application of GRAAL model to the resumption of International Simple Glass alteration, npj Mater. Degrad. 2(1) (2018) 21.
[61] S. Mercado-Depierre, M. Fournier, S. Gin, F. Angeli, Influence of zeolite precipitation on borosilicate glass alteration under hyperalkaline conditions, J. Nucl. Mater. 491 (2017) 67-82.
[62] V. Piovesan, I. Bardez-Giboire, M. Fournier, P. Frugier, P. Jollivet, V. Montouillout, N. Pellerin, S. Gin, Chemical durability of peraluminous glasses for nuclear waste conditioning, npj Mater. Degrad. 2 (2017) 1-10.
[63] S. Gin, X. Beaudoux, F. Angéli, C. Jégou, N. Godon, Effect of composition on the short-term and long-term dissolution rates of ten borosilicate glasses of increasing complexity from 3 to 30 oxides, J. Non-Cryst. Solids 358(18-19) (2012) 2559-2570.

[64] W.L. Bourcier, D.W. Peiffer, K.G. Knauss, K.D. McKeegan, D.K. Smith, A kinetic model for borosilicate glass dissolution affinity of a surface alteration layer., Mater. Res. Soc. Symp. Proc. 176 (1989) 209-216.
[65] I. Munier, J.L. Crovisier, Alteration of Si-B-Na-Al model glass in water at 90 °C: experiments and thermodynamic modelling, Mater. Res. Soc. Symp. Proc. 757 (2003) 153-158.

Appendix A

In the tests conducted in this study, the pH was manually regulated around a set value. Figures A.1 (for the S1 test series) and A.2 (for the S2 test series) show the different set pH values (dashed lines), measured pH values (circles), and pH values reached after addition of micro-volumes of KOH or HNO_3 solutions if necessary (crosses). Mean pH values (m) and standard deviations (σ) are given in the caption.

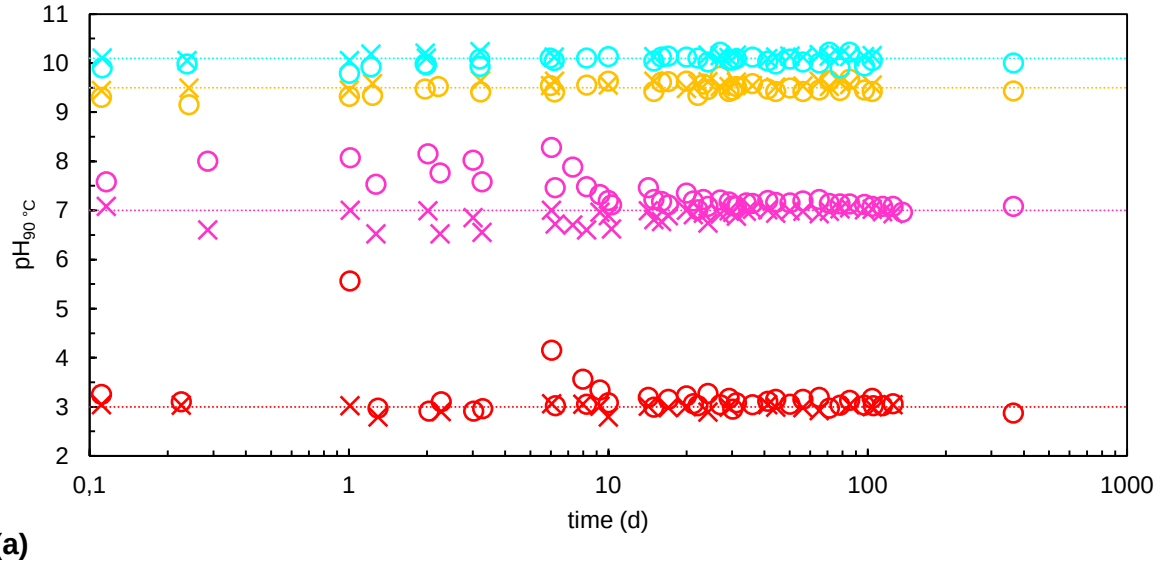

(a)

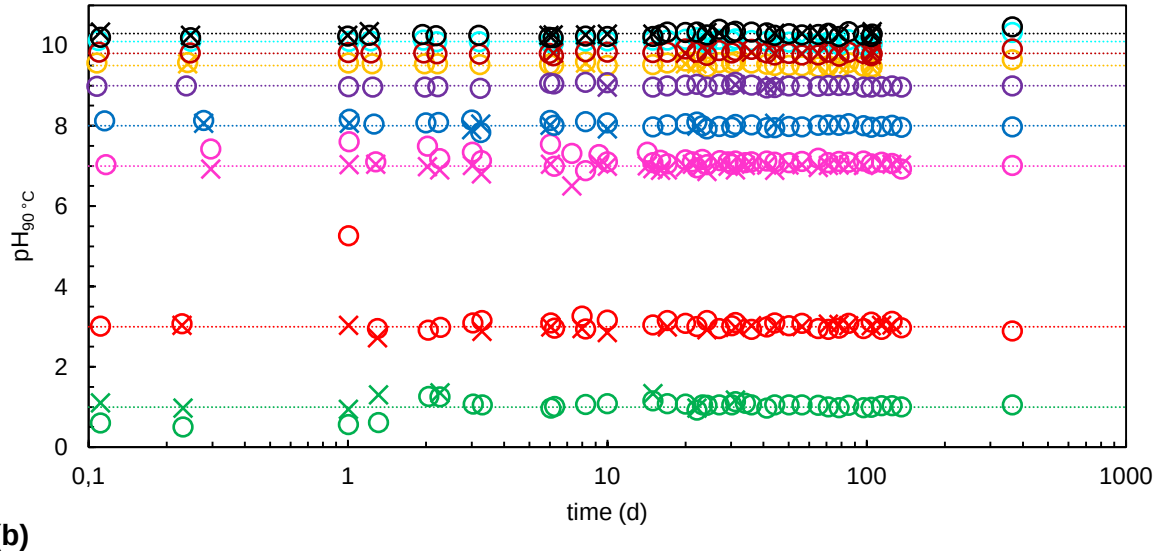

(b)

Figure A.1: pH measured in the S1 **(a)** "Blk" and **(b)** "Sat" test series before regulation (○) and after regulation (×) around set values (dotted lines) of $pH_{90\,°C}$ = 1 (green, m_{sat} = 1.0, σ_{sat} = 0.2), 3 (red, m_{Blk} = 3.1, σ_{Blk} = 0.4, m_{sat} = 3.1, σ_{sat} = 0.3), 7 (pink, m_{Blk} = 7.1, σ_{Blk} = 0.4, m_{sat} = 7.1, σ_{sat} = 0.2), 8 (blue, m_{sat} = 8.0, σ_{sat} = 0.1), 9 (purple, m_{sat} = 9.0, σ_{sat} = 0.0), 9.5 (orange, m_{Blk} = 9.5, σ_{Blk} = 0.1, m_{sat} = 9.5, σ_{sat} = 0.0), 9.8 (dark red, m_{sat} = 9.8, σ_{sat} = 0.0), 10.1 (light blue, m_{Blk} = 10.1, σ_{Blk} = 0.1, m_{sat} = 10.1, σ_{sat} = 0.1), and 10.3 (black, m_{sat} = 10.3, σ_{sat} = 0.1).

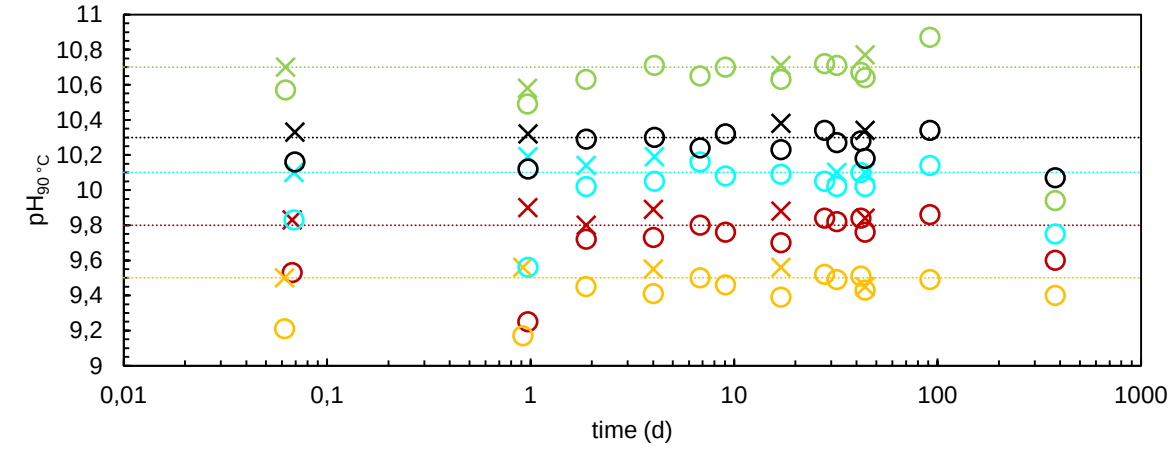

(a)

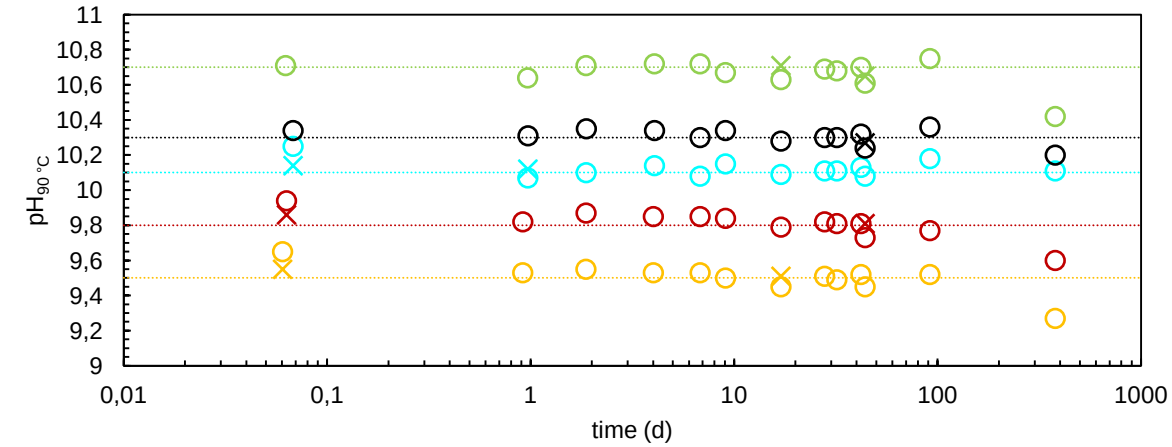

(b)

Figure A.2: pH measured in the S2 **(a)** "Blk" and **(b)** "Sat" test series before regulation (○) and after regulation (×) around set values (dotted lines) of $pH_{90\,°C}$ = 9.5 (orange, m_{Blk} = 9.4, σ_{Blk} = 0.1, m_{sat} = 9.5, σ_{sat} = 0.1), 9.8 (dark red, m_{Blk} = 9.8, σ_{Blk} = 0.2, m_{sat} = 9.8, σ_{sat} = 0.1), 10.1 (light blue, m_{Blk} = 10.0, σ_{Blk} = 0.2, m_{sat} = 10.1, σ_{sat} = 0.0), 10.3 (black, m_{Blk} = 10.3, σ_{Blk} = 0.1, m_{sat} = 10.3, σ_{sat} = 0.0), and 10.7 (light green, m_{Blk} = 10.6, σ_{Blk} = 0.2, m_{sat} = 10.7, σ_{sat} = 0.1).

Appendix B

Zoomed-in subfigures of Figure 3 are shown in Figure B.1.

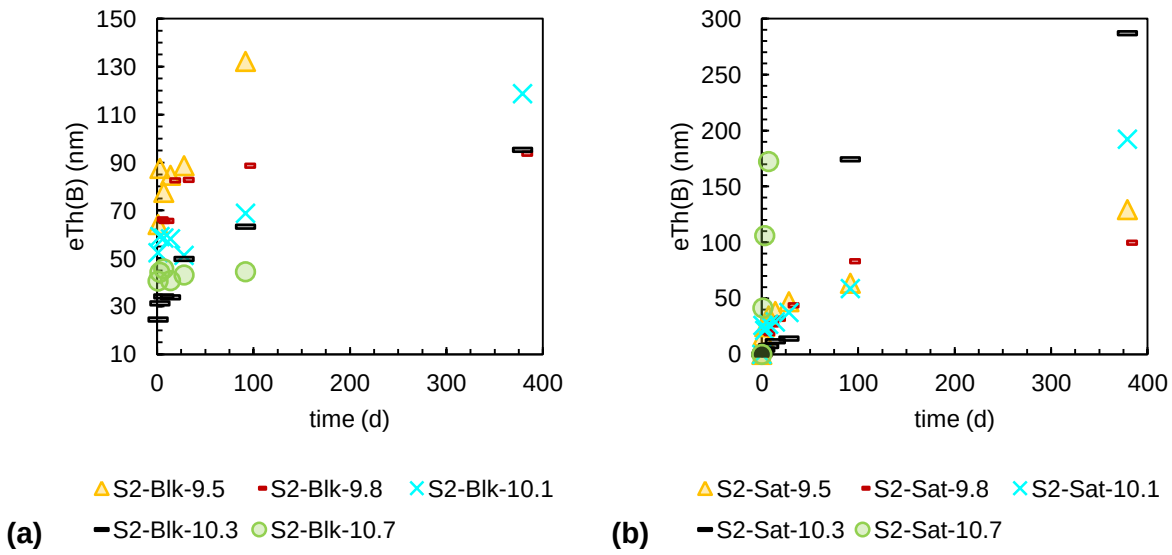

580 **Figure B.1:** Zoomed-in subfigures of **(a)** Figure 3.a and **(b)** Figure 3.b, showing the evolution of the equivalent thickness of altered glass calculated from the boron concentration, eTh(B), for the **(a)** S2-Blk and **(b)** S2-Sat test series with an *S*/*V* ratio of 10 000 m^{-1}.

Appendix C

A direct comparison between the “Blk” and “Sat” tests at all sampling dates is shown in Figures C.1 and C.2.

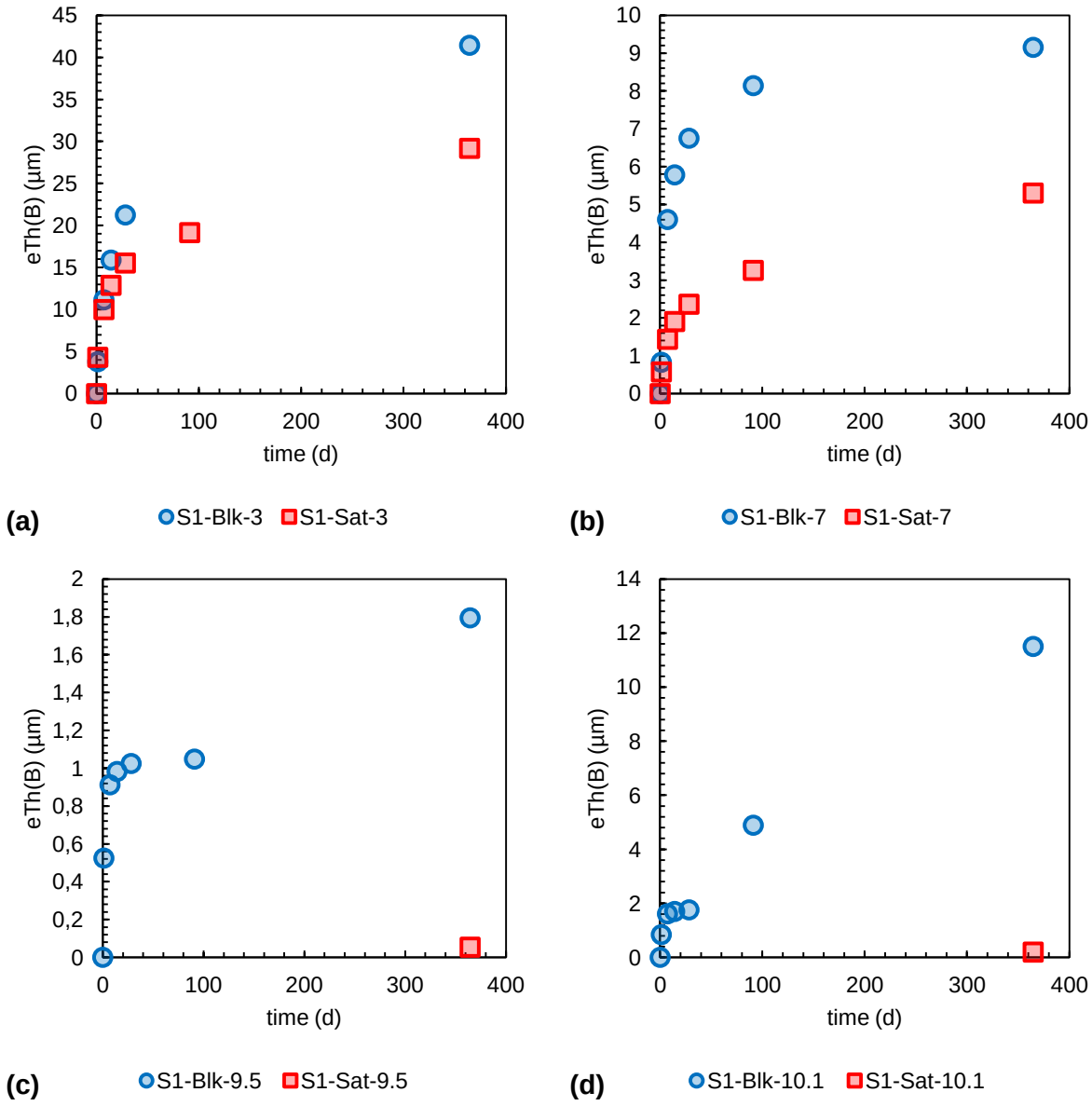

Figure C.1: Comparison of the evolution of the equivalent thickness of altered glass calculated from the boron concentration, eTh(B), for the S1 test series with an *S*/*V* ratio of 60 m^{-1} at $pH_{90\,°C}$ values of **(a)** 3, **(b)** 7, **(c)** 9.5, and **(d)** 10.1.

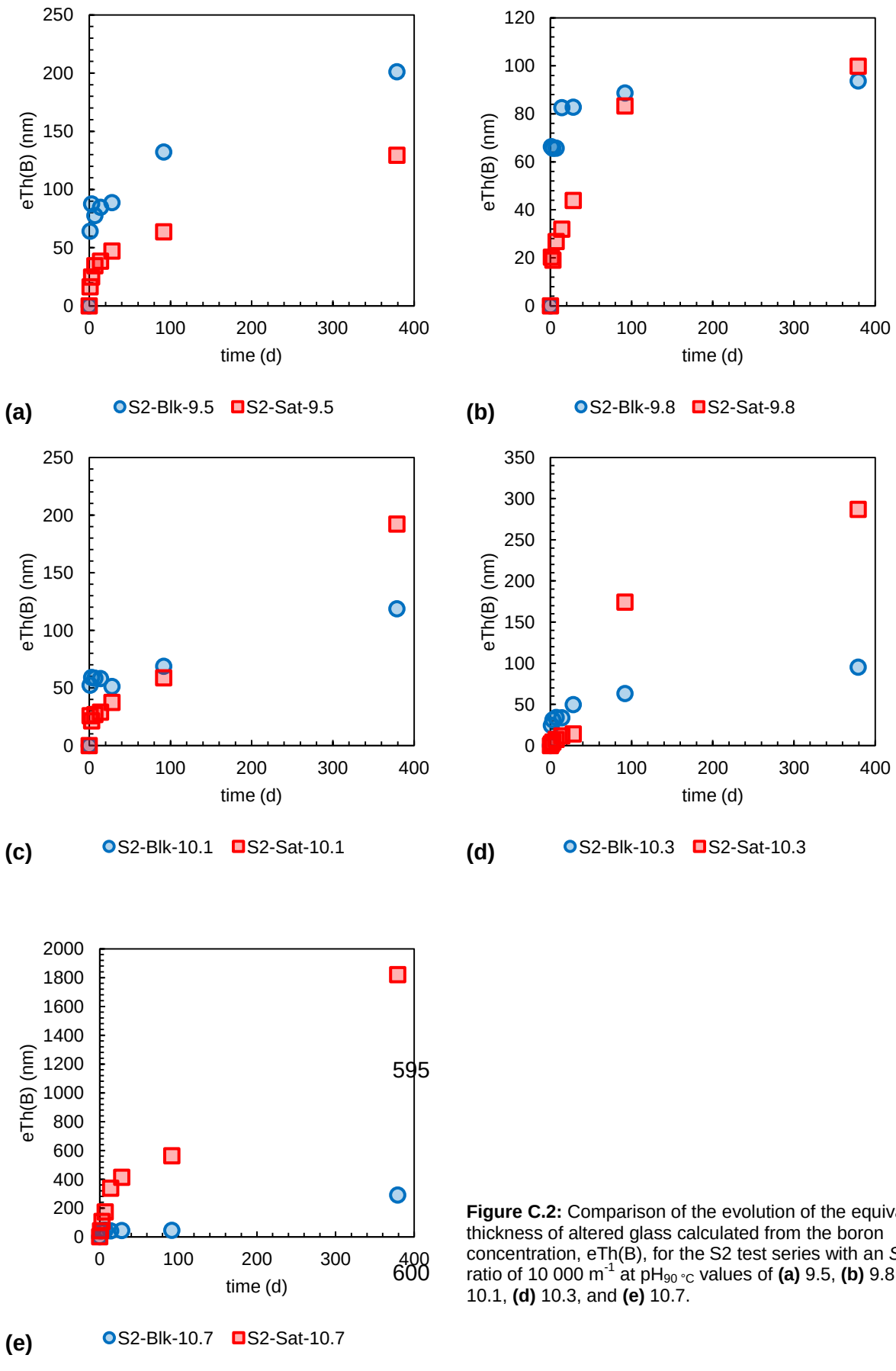

Figure C.2: Comparison of the evolution of the equivalent thickness of altered glass calculated from the boron concentration, eTh(B), for the S2 test series with an *S*/*V* ratio of 10 000 m^{-1} at $pH_{90\,°C}$ values of **(a)** 9.5, **(b)** 9.8, **(c)** 10.1, **(d)** 10.3, and **(e)** 10.7.

Appendix D

The solution concentrations measured in the tests are summarized in the tables in Appendix D in the order given in Table 2 (LoQ: limit of quantification, NA: not analyzed).

D.1. S1-Sat-1

Time (d)	Si (g·m^{-3})	B (g·m^{-3})	Na (g·m^{-3})	Al (g·m^{-3})	Ca (g·m^{-3})	Zr (g·m^{-3})
0.0	307.7	< LoQ	62.7	< LoQ	< LoQ	< LoQ
1.2	288.3	37.4	93.0	1.2	13.7	< LoQ
7.3	308.0	72.0	210.2	1.5	20.5	< LoQ
14.2	343.5	78.5	234.5	1.6	21.0	< LoQ
28.2	487.8	88.0	247.5	2.2	22.4	< LoQ
91.1	585.1	101.7	421.7	4.1	31.1	< LoQ
364.6	558.7	111.5	358.8	4.2	30.3	< LoQ

D.2. S1-Blk-3

Time (d)	Si (g·m^{-3})	B (g·m^{-3})	Na (g·m^{-3})	Al (g·m^{-3})	Ca (g·m^{-3})	Zr (g·m^{-3})
0.0	3.3	< LoQ	< LoQ	< LoQ	< LoQ	< LoQ
1.2	8.4	27.3	45.3	0.8	11.4	< LoQ
7.2	33.0	74.1	128.5	2.7	28.3	< LoQ
14.2	45.9	99.9	170.5	4.8	37.8	< LoQ
28.2	54.5	125.7	217.5	5.7	47.0	< LoQ
91.1	93.1	201.6	324.2	6.5	145.9	< LoQ
364.6	600.1	180.8	326.9	8.3	71.8	< LoQ

D.3. S1-Sat-3

Time (d)	Si (g·m^{-3})	B (g·m^{-3})	Na (g·m^{-3})	Al (g·m^{-3})	Ca (g·m^{-3})	Zr (g·m^{-3})
0.0	298.9	< LoQ	5.5	< LoQ	1.3	< LoQ
1.2	306.5	31.8	57.4	< LoQ	17.0	< LoQ
7.2	320.3	69.2	125.9	< LoQ	25.1	< LoQ
14.2	313.9	86.6	162.0	< LoQ	28.6	< LoQ
28.2	317.9	101.9	195.7	< LoQ	31.2	< LoQ
91.1	361.4	121.5	246.4	< LoQ	74.2	< LoQ
364.6	945.8	172.9	417.1	< LoQ	57.4	< LoQ

D.4. S1-Blk-7

Time (d)	Si (g·m^{-3})	B (g·m^{-3})	Na (g·m^{-3})	Al (g·m^{-3})	Ca (g·m^{-3})	Zr (g·m^{-3})
0.0	2.2	< LoQ	< LoQ	< LoQ	0.7	< LoQ
1.2	17.3	6.0	10.7	0.9	3.1	< LoQ
7.2	58.5	34.3	57.2	< LoQ	11.1	< LoQ
14.2	62.8	42.8	71.9	< LoQ	15.1	< LoQ
28.2	65.9	50.0	86.6	< LoQ	19.3	< LoQ
91.1	76.0	60.2	100.2	< LoQ	50.7	< LoQ
364.6	249.3	67.6	117.4	< LoQ	27.5	< LoQ

D.5. S1-Sat-7

Time (d)	Si (g·m^{-3})	B (g·m^{-3})	Na (g·m^{-3})	Al (g·m^{-3})	Ca (g·m^{-3})	Zr (g·m^{-3})
0.0	146.4	< LoQ	5.6	< LoQ	1.4	< LoQ
1.2	150.8	4.5	12.0	< LoQ	3.3	< LoQ
7.2	139.9	11.6	25.9	< LoQ	7.0	< LoQ
14.2	138.6	15.5	31.2	< LoQ	9.1	< LoQ
28.2	134.6	19.5	39.4	< LoQ	11.2	< LoQ
91.1	177.4	27.5	52.2	< LoQ	27.8	< LoQ
364.6	332.5	45.9	9.6	< LoQ	23.6	< LoQ

D.6. S1-Sat-8

Time (d)	Si (g·m^{-3})	B (g·m^{-3})	Na (g·m^{-3})	Al (g·m^{-3})	Ca (g·m^{-3})	Zr (g·m^{-3})
0.0	175.9	< LoQ	6.1	< LoQ	1.9	< LoQ
1.2	154.5	2.6	8.9	< LoQ	2.1	< LoQ
7.2	154.4	6.4	17.9	< LoQ	5.0	< LoQ
14.2	147.6	7.7	20.8	< LoQ	5.1	< LoQ
28.2	148.5	9.2	23.3	< LoQ	5.9	< LoQ
91.1	164.1	12.0	27.9	< LoQ	12.2	< LoQ
364.6	257.3	16.7	38.6	< LoQ	9.5	< LoQ

D.7. S1-Sat-9

Time (d)	Si (g·m^{-3})	B (g·m^{-3})	Na (g·m^{-3})	Al (g·m^{-3})	Ca (g·m^{-3})	Zr (g·m^{-3})
0.0	276.0	< LoQ	5.6	< LoQ	1.2	< LoQ
1.1	252.0	1.2	6.8	< LoQ	1.2	< LoQ
7.2	276.2	2.2	9.2	< LoQ	1.8	< LoQ
14.2	248.5	2.5	9.9	< LoQ	1.9	< LoQ
28.2	247.1	2.9	10.4	< LoQ	1.9	< LoQ
91.0	283.8	3.7	11.5	< LoQ	10.1	< LoQ
364.6	471.6	5.2	21.3	< LoQ	2.6	< LoQ

D.8. S1-Blk-9.5

Time (d)	Si (g·m^{-3})	B (g·m^{-3})	Na (g·m^{-3})	Al (g·m^{-3})	Ca (g·m^{-3})	Zr (g·m^{-3})
0.0	5.7	< LoQ	0.5	< LoQ	< LoQ	< LoQ
1.1	20.0	4.2	7.8	2.1	2.4	< LoQ
7.2	35.9	7.3	13.4	2.9	2.9	< LoQ
14.2	41.8	7.9	14.8	2.7	2.6	< LoQ
28.2	44.0	8.2	16.0	2.4	2.6	< LoQ
91.0	61.7	8.4	19.8	2.1	10.9	< LoQ
364.6	142.1	15.3	29.6	< LoQ	2.3	< LoQ

D.9. S1-Sat-9.5

Time (d)	Si (g·m^{-3})	B (g·m^{-3})	Na (g·m^{-3})	Al (g·m^{-3})	Ca (g·m^{-3})	Zr (g·m^{-3})
0.0	743.0	< LoQ	11.0	< LoQ	1.2	< LoQ
1.1	641.8	< LoQ	11.2	< LoQ	1.1	< LoQ
7.2	629.2	< LoQ	11.4	< LoQ	0.9	< LoQ
14.2	592.6	< LoQ	10.9	< LoQ	0.8	< LoQ
28.2	546.7	< LoQ	11.6	< LoQ	1.1	< LoQ
364.6	838.2	1.0	20.2	< LoQ	< LoQ	< LoQ

D.10. S1-Sat-9.8

Time (d)	Si (g·m^{-3})	B (g·m^{-3})	Na (g·m^{-3})	Al (g·m^{-3})	Ca (g·m^{-3})	Zr (g·m^{-3})
0.0	1349.5	< LoQ	20.1	< LoQ	3.3	< LoQ
1.2	1192.2	< LoQ	18.7	< LoQ	2.0	< LoQ
7.2	1171.9	< LoQ	20.2	< LoQ	2.0	< LoQ
14.2	1161.8	< LoQ	19.5	< LoQ	1.4	< LoQ
28.2	1013.6	< LoQ	20.3	< LoQ	< LoQ	< LoQ
364.6	1579.0	1.1	29.8	< LoQ	< LoQ	< LoQ

D.11. S1-Blk-10.1

Time (d)	Si (g·m^{-3})	B (g·m^{-3})	Na (g·m^{-3})	Al (g·m^{-3})	Ca (g·m^{-3})	Zr (g·m^{-3})
0.0	23.6	< LoQ	3.1	< LoQ	< LoQ	< LoQ
1.1	35.7	6.3	12.5	3.2	1.8	< LoQ
7.1	66.7	12.3	24.2	5.3	1.4	< LoQ
14.2	66.8	13.0	26.1	5.1	1.3	< LoQ
28.2	75.3	13.5	27.3	4.8	1.2	< LoQ
91.1	138.2	38.3	66.9	2.6	39.4	< LoQ
364.6	510.0	108.0	203.1	0.7	< LoQ	< LoQ

620 **D.12. S1-Sat-10.1**

Time (d)	Si (g·m^{-3})	B (g·m^{-3})	Na (g·m^{-3})	Al (g·m^{-3})	Ca (g·m^{-3})	Zr (g·m^{-3})
0.0	3846.8	< LoQ	49.9	< LoQ	9.7	< LoQ
1.1	3358.4	< LoQ	42.1	< LoQ	< LoQ	< LoQ
7.2	3450.0	< LoQ	47.6	< LoQ	< LoQ	< LoQ
14.2	3406.3	< LoQ	45.8	< LoQ	< LoQ	< LoQ
28.2	2831.7	< LoQ	46.7	< LoQ	6.1	< LoQ
364.6	3966.4	2.5	62.7	< LoQ	< LoQ	< LoQ

D.13. S1-Sat-10.3

Time (d)	Si (g·m^{-3})	B (g·m^{-3})	Na (g·m^{-3})	Al (g·m^{-3})	Ca (g·m^{-3})	Zr (g·m^{-3})
0.0	11844.4	< LoQ	132.4	< LoQ	17.2	< LoQ
1.0	9931.4	< LoQ	114.6	< LoQ	< LoQ	< LoQ
7.1	10724.6	< LoQ	123.7	< LoQ	< LoQ	< LoQ
14.2	9742.5	< LoQ	117.7	< LoQ	< LoQ	< LoQ
28.2	10311.8	< LoQ	128.1	< LoQ	< LoQ	< LoQ
364.6	18112.3	3.1	178.4	4.1	< LoQ	< LoQ
364.6	18112.3	3.1	178.4	4.1	< LoQ	< LoQ

D.14. S2-Blk-9.5

Time (d)	Si (g·m^{-3})	B (g·m^{-3})	Na (g·m^{-3})	Al (g·m^{-3})	Ca (g·m^{-3})	Zr (g·m^{-3})
0.0	4.3	NA	NA	NA	NA	NA
1.1	106.3	93.9	167.3	< LoQ	7.6	NA
3.0	119.1	129.9	193.3	< LoQ	11.4	NA
7.0	126.7	114.1	208.5	< LoQ	11.2	NA
14.0	113.1	125.7	228.2	< LoQ	12.1	NA
28.1	111.2	132.4	254.1	< LoQ	16.0	NA
91.8	79.7	207.3	354.3	< LoQ	8.3	NA
379.0	211.4	322.7	558.0	0.0	7.7	NA

D.15. S2-Sat-9.5

Time (d)	Si (g·m^{-3})	B (g·m^{-3})	Na (g·m^{-3})	Al (g·m^{-3})	Ca (g·m^{-3})	Zr (g·m^{-3})
0.0	$7.2 \cdot 10^{2}$	NA	NA	NA	NA	NA
1.1	106.3	93.9	167.3	< LoQ	7.6	NA
3.0	119.1	129.9	193.3	< LoQ	11.4	NA
7.0	126.7	114.1	208.5	< LoQ	11.2	NA
14.0	113.1	125.7	228.2	< LoQ	12.1	NA
28.1	111.2	132.4	254.1	< LoQ	16.0	NA
91.8	79.7	207.3	354.3	< LoQ	8.3	NA
379.0	211.4	322.7	558.0	< LoQ	7.7	NA

D.16. S2-Blk-9.8

Time (d)	Si (g·m^{-3})	B (g·m^{-3})	Na (g·m^{-3})	Al (g·m^{-3})	Ca (g·m^{-3})	Zr (g·m^{-3})
0.0	2.8	NA	NA	NA	NA	NA
1.1	102.6	94.2	150.8	0.7	9.1	NA
3.0	119.6	93.2	166.5	0.7	9.4	NA
7.0	146.6	93.3	173.6	0.7	26.5	NA
14.0	187.5	119.1	185.9	0.6	9.3	NA
28.1	135.9	119.4	201.8	0.8	10.8	NA
91.8	186.9	164.2	322.1	4.4	21.5	NA
379.0	217.3	219.1	359.7	< LoQ	4.5	NA

D.17. S2-Sat-9.8

Time (d)	Si (g·m^{-3})	B (g·m^{-3})	Na (g·m^{-3})	Al (g·m^{-3})	Ca (g·m^{-3})	Zr (g·m^{-3})
0.0	$1.8 \cdot 10^3$	NA	NA	NA	NA	NA
1.1	1200.1	29.9	55.1	< LoQ	12.0	NA
3.0	1149.0	28.0	76.1	< LoQ	9.5	NA
7.0	1200.3	40.5	97.9	< LoQ	21.7	NA
14.0	1288.9	49.0	112.3	< LoQ	20.4	NA
28.1	1086.7	69.4	156.3	< LoQ	19.6	NA
91.8	944.9	259.1	491.1	< LoQ	11.5	NA
379.0	954.7	401.3	766.0	< LoQ	36.7	NA

D.18. S2-Blk-10.1

Time (d)	Si (g·m^{-3})	B (g·m^{-3})	Na (g·m^{-3})	Al (g·m^{-3})	Ca (g·m^{-3})	Zr (g·m^{-3})
0.0	2.1	NA	NA	NA	NA	NA
1.1	148.2	79.0	137.5	1.3	6.6	NA
3.0	161.6	89.3	162.3	1.6	4.3	NA
7.0	157.0	88.3	169.6	1.5	6.5	NA
14.0	149.6	87.8	150.0	1.2	7.2	NA
28.1	139.9	76.1	146.3	1.1	4.2	NA
91.8	190.6	106.7	209.4	0.8	6.6	NA
379.0	323.9	201.4	363.9	< LoQ	3.4	NA

D.19. S2-Sat-10.1

Time (d)	Si (g·m^{-3})	B (g·m^{-3})	Na (g·m^{-3})	Al (g·m^{-3})	Ca (g·m^{-3})	Zr (g·m^{-3})
0.0	$3.8 \cdot 10^3$	NA	NA	NA	NA	NA
1.1	3454.8	35.5	100.9	< LoQ	30.3	NA
3.0	3411.8	29.0	114.7	< LoQ	40.6	NA
7.0	3558.2	36.7	145.7	< LoQ	50.4	NA
14.0	3297.4	39.7	145.6	< LoQ	35.4	NA
28.1	345.7	52.0	167.5	< LoQ	35.3	NA
91.8	3022.5	83.4	209.1	< LoQ	26.2	NA
379.0	2072.5	283.6	549.0	< LoQ	4.0	NA

D.20. S2-Blk-10.3

Time (d)	Si (g·m^{-3})	B (g·m^{-3})	Na (g·m^{-3})	Al (g·m^{-3})	Ca (g·m^{-3})	Zr (g·m^{-3})
0.0	3.0	< LoQ	< LoQ	< LoQ	< LoQ	NA
1.1	110.2	36.4	79.9	4.6	6.0	NA
3.0	122.7	46.6	94.6	4.3	6.7	NA
7.0	132.1	51.1	100.5	4.4	3.7	NA
14.0	121.6	50.5	110.4	3.6	3.6	NA
28.1	172.6	77.0	148.2	2.9	6.3	NA
91.8	199.4	100.0	187.9	2.1	5.3	NA
379.0	348.5	160.6	289.8	< LoQ	2.3	NA

D.21. S2-Sat-10.3

Time (d)	Si (g·m^{-3})	B (g·m^{-3})	Na (g·m^{-3})	Al (g·m^{-3})	Ca (g·m^{-3})	Zr (g·m^{-3})
0.0	$1.1 \cdot 10^4$	NA	NA	NA	NA	NA
1.1	10143.0	3.1	255.1	< LoQ	14.4	NA
3.0	9411.5	6.4	316.2	< LoQ	32.9	NA
7.0	9389.4	11.1	507.9	< LoQ	35.1	NA
14.0	10201.7	17.5	592.7	< LoQ	57.2	NA
28.1	8601.0	21.2	405.8	< LoQ	20.8	NA
91.7	7977.4	268.2	622.4	< LoQ	54.3	NA
379.0	11372.4	499.9	1170.3	15.9	116.4	NA

D.22. S2-Blk-10.7

Time (d)	Si (g·m^{-3})	B (g·m^{-3})	Na (g·m^{-3})	Al (g·m^{-3})	Ca (g·m^{-3})	Zr (g·m^{-3})
0.0	6.8	NA	NA	NA	NA	NA
1.1	182.3	59.2	124.8	9.6	7.3	NA
3.0	199.2	64.6	132.4	10.6	10.9	NA
7.0	232.3	66.8	138.8	9.8	10.1	NA
14.0	192.3	59.0	123.7	8.9	7.3	NA
28.1	219.2	62.9	128.9	8.3	8.7	NA
91.8	223.6	65.1	138.9	9.8	4.1	NA
379.0	523.4	494.5	845.0	< LoQ	1.9	NA

D.23. S2-Sat-10.7

Time (d)	Si (g·m^{-3})	B (g·m^{-3})	Na (g·m^{-3})	Al (g·m^{-3})	Ca (g·m^{-3})	Zr (g·m^{-3})
0.0	$3.5 \cdot 10^4$	NA	NA	NA	NA	NA
1.1	27212.2	58.7	532.6	17.5	54.8	NA
3.0	28906.7	149.8	752.3	22.4	57.9	NA
7.0	24827.6	243.0	796.5	23.5	71.1	NA
14.0	24505.0	471.5	1178.2	23.9	55.3	NA
28.1	24983.9	574.2	1357.2	23.7	< LoQ	NA
91.7	24054.0	772.2	1722.1	19.1	64.2	NA
379.0	25165.1	2502.4	5243.9	29.5	30.9	NA